Development and Plausibility Assessment of an Active Human Body Model in Numerical Cyclist to Vehicle Collision Simulations based on Real-life Accident Data

Niclas Trube, Patrick Lerge, Lennart V. Nölle, Jörg Mönnich, Thomas Lich, Syn Schmitt

Abstract Finite element (FE) human body models (HBMs) have been used in the past to investigate injury biomechanics of road users in simulations based on accident data and were validated with postmortem human subject data. Recent HBM developments increasingly implement activatable musculature in both occupant and pedestrian applications because they show a significant difference in kinematics and injury biomechanics compared to passive HBMs (PHBMs). In this study, an active FE HBM (AHBM) was developed by incorporating 658 controlled Hill-type muscles adapted from a scalable muscle driven multibody HBM into the Total HUman Model for Safety (THUMS^{TM}) V4.02 AM50 Pedestrian, allowing for stabilisation of the pre-impact position and for the assessment of muscle injuries. Using a previously developed method, multiple accident cases were replicated numerically and model prediction of kinematics, collision points and injuries were compared to the accident case documentation and to the PHBM results. The AHBM results agreed very well with the accident data overall, but not as well as the PHBM in terms of injury prediction. Strain-based injury assessment for the pelvis further suggests that the femoral head's position in the acetabulum is not entirely physiologically valid, which should be considered in future HBM and AHBM development.

Keywords Muscle modelling, muscle injury assessment, active human body model, accident reconstruction, cyclist to vehicle collision

I. INTRODUCTION

Recent traffic accident statistics show that the number of bicycle accidents has not been decreasing in the EU [1, 2] and that the majority of cyclist fatalities results from collisions with passenger cars [3]. Finite element (FE) human body models (HBMs) have been used in the past to investigate injury biomechanics of road users in simulations in vehicle collisions [4–6] that were partly compared to real-life accidents [7, 8]. Besides several other HBMs that are available for pedestrian load cases [9–11], the Total HUman Model for Safety (THUMS^{TM}) V4.02 AM50 Pedestrian [12], which has been validated [13] based on experimental data from generic vehicle collisions with postmortem human subjects (PMHSs) [14, 15], can be used for these kinds of accident reconstructions. This is especially interesting for load cases, such as cyclist to vehicle collisions, for which validation is currently not possible due to a lack of PMHS data in the literature. In general, it has been discussed in the past, whether validation of numerical model predictions with experimental data is even possible in the first place, such as an HBM validation based on experimental PMHS data, or if the term "comparison with experiments" would be more appropriate [16–19]. A previously published method of accident reconstruction using HBMs allows for a comparison of numerical collision simulation with real-life accident data, thus gaining trust in the model predictions [20].

As shown in previous studies, the behaviour of pedestrians and cyclists differ and must be considered separately in traffic safety assessment [21, 22]. Real-life accident data, despite having more unknown or imperfect data available than experimental PMHS validation data, offer the opportunity to compare simulation results and injury predictions with reality for comparable accident cases involving vulnerable road users (VRU).

Recent HBM developments increasingly implement activatable musculature in both occupant [23] and pedestrian applications [24–26] because they show a significant difference in kinematics and injury biomechanics compared to passive HBMs (PHBMs) [27].

In this study, a previously developed method for plausibility assessment of numerical VRU collision simulation in comparison to accident data [20] is applied. The method of the previous study [20] was extended for this work

N. Trube (e-mail: niclas.trube@emi.fraunhofer.de, phone: +49 761 2714-394) is a Research Fellow at Fraunhofer Institute for High-Speed Dynamics (EMI), Germany. P. Lerge and L.V. Nölle are Ph.D. researchers, S. Schmitt is Professor for Computational Biophysics and Biorobotics at the Institute for Modelling and Simulation of Biomechanical Systems of University of Stuttgart, Germany. J. Mönnich and T. Lich are Accident Research Specialists at Robert Bosch GmbH, Germany.

by implementing active musculature [28–32] into the Total HUman Model for Safety (THUMS™) V4.02 AM50 Pedestrian[1], which was repositioned into an average cyclist posture [22]. Muscle routing and muscle parameterisation were adopted from a scalable multi body HBM based on [33–36]. To determine the appropriate muscle activity for the simulated scenario, a forward dynamic multibody simulation was performed with demoa [37] using the model adapted to the dimensions of the THUMS, with the joint angles of the cyclist's posture applied to the HBM as controller specifications [38]. The muscle activity was then derived after successfully achieving the force equilibrium to hold the expected posture. Finally, the muscle activity was applied to the THUMS model via the muscle material interface as a time-constant control variable, resulting in an active human body model (AHBM) with additional active joint stiffness.

Using this newly developed AHBM, a plausibility assessment [20] was performed, thus reconstructing single accident cases obtained from the German In-Depth Accident Study (GIDAS) [39, 40] in the previously developed simulation setup [20]. Hereby, the predicted collision points, injury-inducing contact pairs, as well as injuries were compared with their respective counterpart in the GIDAS documentation. Further, this allowed for a comparison of the previously published results of the PHBM [20] with the newly developed AHBM.

To the best knowledge of the authors, this is the first study utilising an FE AHBM in numerical accident reconstructions of bicycle to car collisions. Furthermore, the comparison of muscle injuries as part of a whole-body injury and contact assessment has added new information to the field of crash simulation and AHBM plausibility assessment.

II. METHODS

This study has been conducted as part of the national research project *Artificial Intelligence for Real-Time Injury Prediction (ATTENTION)*. The aim of *ATTENTION* is to develop a method for real-time injury prediction of VRUs, such as pedestrians or cyclists as part of a proof-of-concept study. For this purpose, data-driven methods have been used to determine a situation-specific injury risk from vehicle-based video data and virtual tests with the help of FE HBMs. Prospectively, the Artificial Intelligence (AI) based injury prediction shall enable both safe and efficient traffic through automated vehicle risk mitigation strategies. An efficient method for data generation in this context was previously published [41]. Further, a study on the extraction of a mean cyclist-position from vehicle-bound video documented car-cyclist collisions was published [21, 22]. This mean cyclist-position was used as described in a previous study on cyclist plausibility assessment [20] and is used in the same way in this study.

As previously described [20], creating individual bicycle models, car models (including the verification of the windscreen) or individualised HBMs as a direct counterpart of the vehicles and VRUs involved in the single GIDAS cases is not intended and would exceed the scope of the project. Considering this limitation, we developed a virtual setup for collisions, where the cyclist collided with the car front end. Each component (car, bicycle and cyclist) was compared to or developed based on data from the GIDAS database to allow for a comparison between the results from numerical cyclist to vehicle collision simulations and real-world collision data [20].

Accident Case Selection

The three GIDAS cases[2] used for comparison with numerical data resulted from filtering according to the dimensions of the publicly available Toyota Camry vehicle model (Table I, Fig. 1) [42] and to the body size and weight of the THUMS (Table II) [12]. Further, only cases were selected where a frontal vehicle-to-cyclist collision was documented with a large number of injuries. Further details on the accident case selection, accident documentation, as well as the process of comparing numerical simulation and accident data regarding various aspects are provided in a previously published paper on passive cyclist plausibility assessment [20]. This previous work also included the development of an FE bicycle model (A-Fig. 6) based on the average GIDAS bicycle dimensions and the modification of the Toyota Camry vehicle model for VRU load cases by incorporating a windshield model validated for VRU applications [20, 41].

[1] Throughout only the abbreviation “THUMS” will be used for the Total HUman Model for Safety (THUMS™) V4.02 AM50 Pedestrian used in this study.
[2] In this study, the GIDAS documentation of accident cases with the IDs 1050918, 1170986 and 30090880 were compared with simulation data.

TABLE I
COMPARISON OF THE FE CAR MODEL WITH THE GIDAS PASSENGER CARS [20]

#GIDAS	#car	Mass [kg]	H1 [cm]	H2 [cm]	H3 [cm]	L1 [cm]	L2 [cm]	L3 [cm]
-	Camry	1603.8	77.1	99.9	136.2	12.2	111.4	185.0
1050918	car1	1530±[3]73.8	70.0±7.1	92.4±7.5	131.6±4.6	11.0±1.2	108.9±2.5	175.6±9.4
1170986	car2	1575±28.8	73.2±3.9	96.1±3.8	138.1±1.9	10.4±1.8	107.3±4.1	186.8±1.8
30090880	car3	1146±457.8	75.4±1.7	96.0±3.9	134.8±1.4	16.6±4.4	106.7±4.7	175.0±10

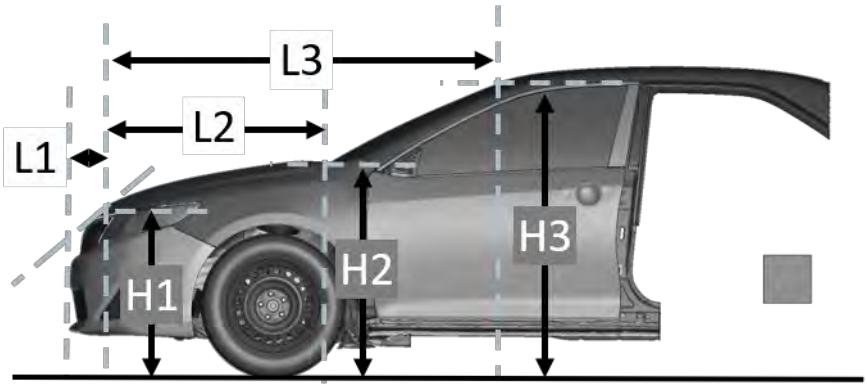

Fig. 1. Vehicle dimensions compared between the adapted FE model and the GIDAS cars in Table I. The FE model [42] was modified in terms of a load-case specific reduction and an adaption of the windshield [20].

TABLE II
COMPARISON OF THUMS TO THE GIDAS CYCLISTS [20]

#GIDAS	Weight [kg]	Standing Height	Age
THUMS	77.2	178.2	-
1050918	75±2.2	177±1.2	32
1170986	80±2.8	180±1.8	33
30090880	81±3.8	174±4.2	56

Development of the FE AHBM

To activate the passive THUMS HBM [9] 1D beam muscles [28–32] were implemented into the model. To determine the respective muscle origins, insertions, and deflection points, first, a scalable multibody (MB) HBM based on [33–36] was anthropometrically and kinematically adjusted to fit to size and posture of the THUMS. Estimated positions and orientations of the FE HBM joint axes were used as references for the adjustment process. Joint locations and their axis orientations as well as the segment length in between were estimated geometrically in advance based on the default upright standing FE PHBM. The MB HBM has a total of 658 muscles, which are deflected up to two times using via-point routing, and the muscle material [29, 43, 44] available is, based on its theory, identical to the FE muscle material [28–32].

Subsequently, the 3D locations of all muscle origins, insertions, and deflection points, as well as the locations and orientations of each body's centre of gravity were exported from the MB model and transformed into new node sets for the FE HBM using a MATLAB® (Mathworks, Natick, MA, USA) [45] based pre-processing script. In this process, all implementations were done via additional module files. The HBM base file itself was not edited. Afterwards, the FE HBM was repositioned as described in a previous study [20] according to the determined cyclist pose [22], together with the new nodes of the muscle and segment orientation instrumentation. The required angles used in OASYS Primer (Oasys Ltd, London, United Kingdom) [46] for repositioning were determined using the repositioned multibody model as reference, as the default THUMS pedestrian was not set up in a neutral zero pose [47]. The target angles determined in this way are listed in TABLE A-V in the Appendix.

In the next processing step, the actual local joint angle kinematics of the repositioned THUMS model were

[3] In contrast to the common usage of "±" symbol as the margin of error, the symbol was used in Table I and Table II to uniformly define a positive or negative divergence from the FE model dimensions.

determined from the local body orientation systems, which were adopted as coordinate nodes from the MB model. The MB AHBM was then repositioned accordingly. After that, a forward dynamic simulation with 5 seconds of simulation time was done in which the initial joint angle position was used as a controller input to a hierarchical muscle controller [38] which had to control actively against the influence of gravity on the body. This way, the muscle activity necessary to hold the body in the current position was determined. This was achieved by generating a torque equilibrium in the joints based on acting muscle forces. It is necessary to mention that the muscular activity and not the stimulation signal [32] was determined and transferred as control input from the MB simulation environment demoa to LS-DYNA. This skips the activation time in the activation dynamics of the muscle, as a pre-activated muscle is assumed. As the final force equilibrium was reached after 5 seconds of simulation, the mean values of the muscular activity from the last 500 ms of the pre-simulation with demoa [37] were then transferred and included in the FE HBM as load curve with constant level in order to filter slight but constant oscillations in the signal. In addition, the muscle implementation was completed by providing the remaining keywords required for the muscle implementation, particularly the material cards, as modules for the FE AHBM. For the generic muscle parameters, the standard values [48] were used. Length- and force related parameters were adjusted to the THUMS based on a previously described scaling procedure [31].

When applying the pre-computed muscles to the FE AHBM, it was found that the muscular contraction forces initially resulted in a settling behaviour of the joint contact surfaces. This led to translational movements of up to 7 mm, for example, at the contact interface between the femoral head and the acetabulum, closing the pre-existing joint gaps. A comparable translational movement did not take place in the MB AHBM, as the joints were predefined in that case. This unwanted settling behaviour of the FE AHBM due to a lack of proper model calibration led to a lower tensile force applied by the muscles and a lower joint stiffness than in the precomputed MB AHBM. As we have only studied a fixed pose with constant activity, however, there was only a slight rotational change in the target position of the FE AHBM after the translation. For an intended active, actual movement, model calibration of the FE AHBM is mandatory, because otherwise the simulated kinematics of the FE AHBM would deviate from the expected path predicted in the MB simulation. In test simulations without vehicle contact, it was noticeable that the muscles successfully contributed to the stabilisation of the cyclist on the bike. The same behaviour also occurred for contacts with low collision speeds. In this respect, the contact behaviour of the cyclist FE AHBM corresponds more to that of a real VRU than the passive FE HBM. The relevant data and keyfiles to reposition the THUMS into a cyclist position, compatible with the bicycle model of this work, and to implement muscle elements accordingly are provided via the Darus repository [49].

Muscle Strain Injury Assessment

The assessment of muscle strain injury (MSI) severity was performed using the Muscle Strain Injury Criterion (MSIC) developed in a previous study [50]. This injury criterion is based on comparing the force occurring in the muscle-tendon-unit (MTU) F_{MTU} to three force-based threshold curves indicating minor, major and rupture injury of the muscle body. The thresholds are defined in relation to the muscle's tensile failure force F_{tf} which can be calculated using Eq. 1.

$$F_{tf} = 3\,F_{max} \qquad \text{(Eq. 1)}$$

Where F_{tf} is the muscle's tensile failure force and F_{max} is the muscle's maximum isometric force. To account for the varying states of muscular activity and their impact on the injury resistance of the muscle [51], the thresholds are linearly interpolated according to Eq. 2.

$$F_{thres}(a) = F_{thres,pa} + a\left(F_{thres,ac} - F_{thres,pa}\right) \qquad \text{(Eq. 2)}$$

Where F_{thres} is the muscle injury threshold force, $F_{thres,pa}$ is the passive muscle injury threshold, $F_{thres,ac}$ is the active muscle injury threshold and a is the muscular activity between 0 and 1. The specific injury thresholds and a more detailed explanation of the MSIC have previously been published [50].

The MSI assessment was performed for two reasons. The first reason was, to establish if the muscle elements introduced into the base THUMS cyclist model were parameterised correctly and would not create unphysiologically high forces in the model's default posture through a large pre-straining of the muscles.

Unphysiologically high forces in the initial model position would be classified as injuries by the applied injury assessment method. Thus, we used the injury assessment to double-check the initial body pose. For this reason, a simulation without any collision (*no collision simulation*) was performed and the resulting muscle forces were evaluated, which showed that out of the 658 newly introduced muscle elements, only 12 muscles were marked as injured. All marked muscles were located in the hip and lower back regions of the cyclist model (A-Fig. 11). Given that these body regions were highly deformed during the repositioning of the PHBM using Oasys PRIMER (Oasys Ltd, London, United Kingdom) [46], the high strains can be explained not in terms of poor parameter choice but in terms of PHBM defects. Joint gaps, which had been widened during the repositioning, cause large initial muscle strains which only subside once the musculature has closed the joint gaps through contraction. As these 12 marked muscles would always show signs of injury, independent of the load case, they were denoted as "baseline injuries". All following strain injury analyses will be described in terms of additionally injured muscles, barring these baseline injuries. Based on these results, the introduced muscular system and its parameterisation were deemed acceptable for the use in the following impact simulations.

Second, the strain injury assessment was performed to determine the quality of the internal force transfer characteristics of the model and to confirm possible minor injuries mentioned in the GIDAS case documentation, which are not covered by the previously outlined statistical and deterministic injury criteria.

The MSI assessment results are listed in Table III. A visualisation of the locations of the injured muscles is provided in A-Fig. 11.

TABLE III
MSI ASSESSMENT RESULTS

#GIDAS	#Injured muscles including baseline injuries	#Injured muscles excluding baseline injuries
1050918	42	30
1170986	74	62
30090880	97	85

The results of the MSI assessment show that the number and location of injured muscles (A-Fig. 11) corresponds to the deterministic injury prediction (Table A-I to A-III) in the respective body regions, as further discussed in the corresponding subsection for each GIDAS case in the discussion section. The increase in the number of injured muscles from *Case 1050918* to *1170986* to *Case 30090880* most likely originates from the observed AHBM kinematics (A-Fig. 1 to A-Fig. 3). For cases with higher amounts of muscle injuries, the AHBM was rather falling with its back on the vehicle exterior. As the spine has been modelled with the highest amount of muscle elements compared to the other body regions, the likeliness of an increase in the number of injured muscles is higher for impacts of the AHBM backside. Additionally, the body regions in which injuries occur match the impact locations between cyclist and car well. This indicates that the model internal force transfer is working as intended, as regions with high external force intake show corresponding signs of internal tissue strain.

HBM Instrumentation and Injury Prediction

The THUMS was instrumented in order to obtain information regarding collision points and several injury criteria. Contact force transducer pairs were implemented to extract contact forces between VRU body regions and vehicle components for a measurable comparison of injury-relevant contact pairs between the accident data and the simulation, in addition to the subjective visual evaluation of collision points. Both, probabilistic and deterministic injury assessment was considered for a holistic comparison with the accident data. Further details regarding the selected injury criteria have been provided in a previous work [20]. Additionally, the implemented muscle system allows for assessment of muscle strain injuries based on a previously developed method applicable for AHBMs [50].

One of the injury criteria evaluated in this study is the strain-based pelvis fracture criterion [52]. The injury values of this criterion are the 95th and 99th percentile values of the maximum principal strain (MPS) distribution (MPS95 and MPS99), which consider the maximum MPS values of each cortical pelvis element over time. Based on an initial evaluation of whole-body injury risk over 400 ms simulation time in the *no collision simulation*, the results showed that muscle contraction leads to an unphysiological injury risk for this pelvis MPS criterion of

AIS2+$_{MPS95}$=34.3 % and AIS2+$_{MPS99}$=60.1 % (Table A-IV, A-Fig. 10) even without a collision. There were no significant injury risks found in the other body regions (A-Fig. 10). The unphysiological injury risk in the pelvis results from a combination of the anatomy of the THUMS and the contraction of the implemented muscle system. THUMS was provided with a gap of 6-8 mm between the femoral head and the acetabulum, which is neither found in the human body nor in the multi-body model described in the subsection *Development of the FE AHBM*. As an effect of the muscular activation in the FE AHBM, the muscle contraction in THUMS led to the femoral head being pulled in medial-proximal direction towards the acetabulum. As this occurs within a few hundred milliseconds for both the *no collision simulation* and collision simulations, this dynamic effect leads to additional strains in elements of the acetabulum and the adjacent pelvis regions, resulting in the beforementioned pelvis injury risk even without a vehicle collision. To allow for a pelvis MPS-based injury assessment with the AHBM in this study nevertheless, the calculation of the injury values was adapted (Eq. 3) for both MPS95 and MPS99 to account for the effect of additionally muscle-driven pelvis strain:

$$MPS95 = MPS95\_collision - MPS95\_no\_collision, \quad \text{(Eq. 3)}$$

where $MPS95$ is the 95th percentile of the maximum principal strain distribution considering the maximum MPS values of each cortical pelvis element over time, $MPS95\_collision$ is the injury value calculated from the simulation with collision (different for each GIDAS case) and $MPS95\_no\_collision$ is the injury value calculated from the simulation without collision (Table A-IV). All MPS values are calculated over the simulation time of 400 ms.

Collision Setup and Simulation Environment

The previously published simulation setup [20] was used in this study. Based on the data collected from individual GIDAS accidents, a previously published simulation matrix (Table IV) was established for left-sided impacts, where the cyclist travelled from the passenger side (right front end) to the driver side (left front end) of the vehicle. An averaged deceleration value of 3.5 m/s² was applied to the front axis of the modified car model for all simulations. This averaged deceleration value was calculated from GIDAS data based on a previous filtering of accident cases, where frontal collisions of passenger cars with cyclists and pedestrians were documented. The collision angle and Y-Offset of each simulation are defined as shown in Table IV. A reference image is shown in Fig. 2. The global coordinate system and the Y-Offset of the simulation setup are defined based on specifications in European New Car Assessment Programme (Euro NCAP) TB024 [53]. For a Y-Offset of 0 mm, the centre of gravity of the THUMS head was aligned with the vehicle centreline.

TABLE IV
PARAMETER DEFINITIONS OF COLLISION SIMULATION BASED ON GIDAS [20]

#GIDAS	Car Velocity [km/h]	Cyclist velocity [km/h]	Y-Offset [mm]	Collision angle [°]
1050918	47	25	-750	226
1170986	30	12	-50	288
30090880	38	5	-100	274

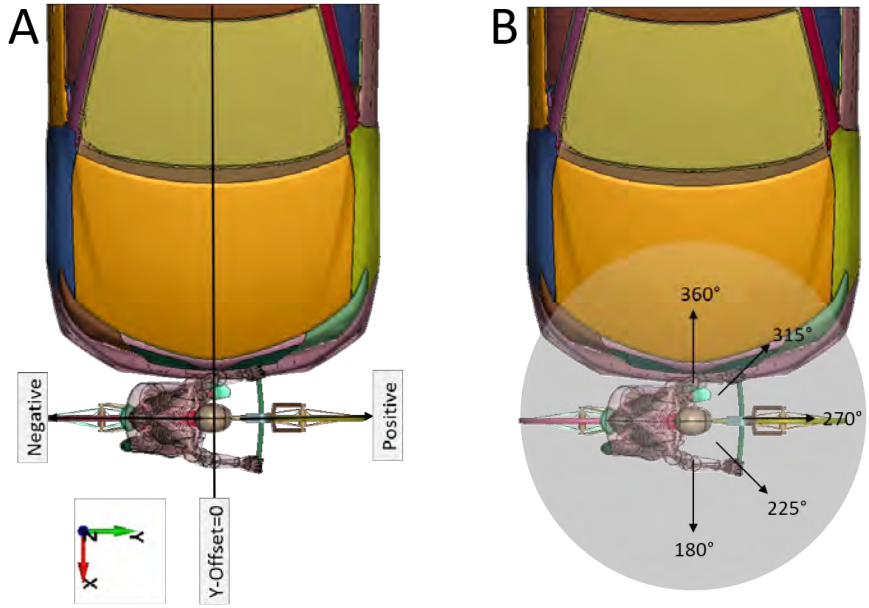

Fig. 2. Definition of the Y-Offset from the vehicle centreline (A) and of the collision angle (B) [20].

III. RESULTS

The results on kinematics, collision points, contact pairs and injury assessment are compared in the following subsections for the PHBM and AHBM and, where possible, with the GIDAS documentation. Additional details on the following results are provided in the discussion to avoid repetition with the results section and to facilitate readability and understanding of the different data being compared.

Kinematics

The whole-body kinematics of case 1170986 are shown in Fig. 3 for the total simulation time of 400 ms with each image being 100 ms apart. The same information is provided for the other cases in the Appendix (A-Fig. 1 to A-Fig. 3). As the GIDAS accident database does not currently contain video information of the accident, a direct comparison of the HBM kinematics presented with GIDAS was not possible. However, an approximation of this type of comparison is provided in the following subsection on collision points.

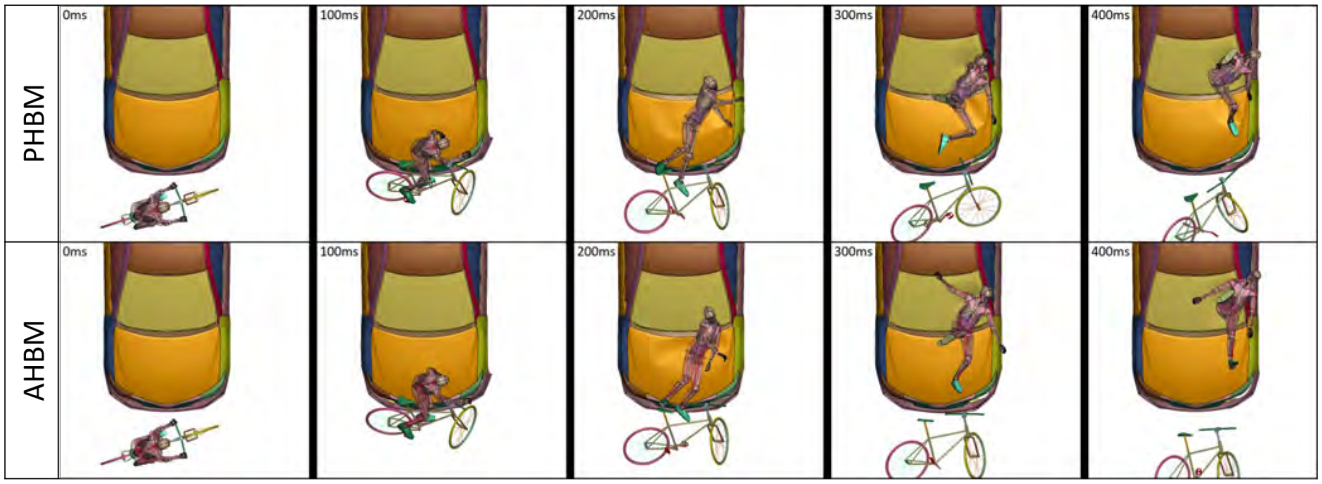

Fig. 3. Exemplary comparison of the whole-body kinematics of the FE collision simulation for case 1170986. The presented data of the PHBM was previously published [20].

Collision points

The collision points between the cyclist and the vehicle model were visually evaluated for the FE simulation (Fig. 4, A-Fig. 4). If available, collision points from the real-life collision were extracted from the GIDAS documentation. Data were missing for GIDAS case 300090880 and were reconstructed based on dents in the

bodywork, observable via photographs in the single case documentation.

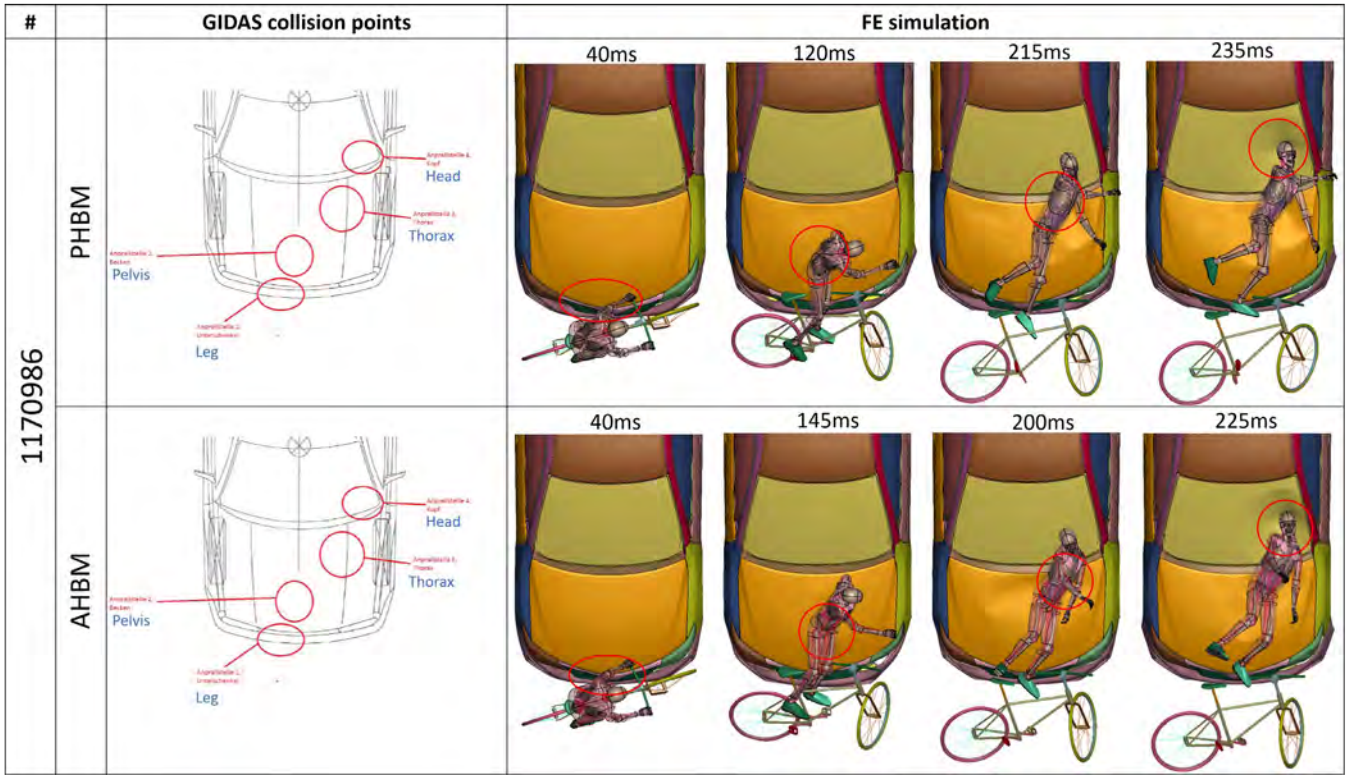

Fig. 4. Exemplary data on the collision points of the cyclist and the vehicle from the accident data and from the collision simulation regarding the documented body regions for case 1170986. English translations were added in blue based on the original image file from GIDAS. The presented PHBM data was previously published [20].

Contact pairs

By defining multiple contact pairs for different combinations of body regions and vehicle components, it was possible to compare injury-inducing contact pairs between GIDAS and the collision simulation (Fig. 5, A-Fig. 5). For example, in case 1170986, peaks in the contact force of the contact force transducer pairs *bumper to left leg* and *windshield to head* could be observed, where extremity injuries due to bumper contact and head injuries due to windshield contact were documented in GIDAS.

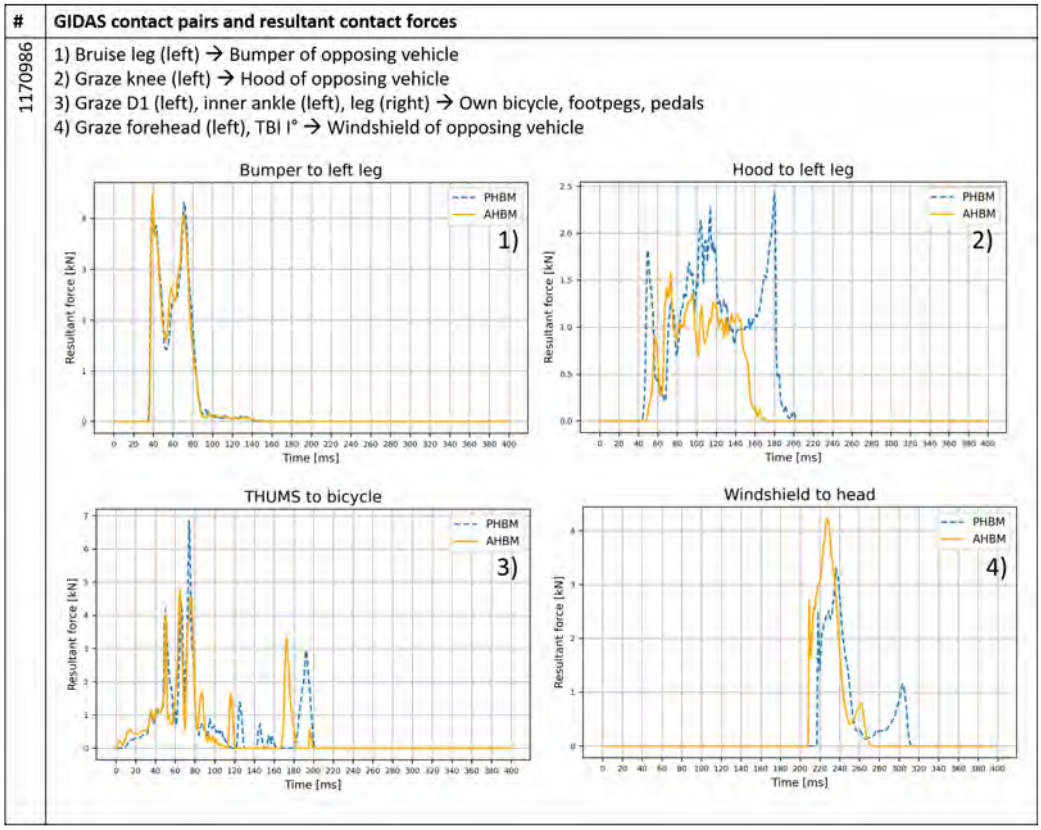

Fig. 5. Exemplary comparison of the injury-causing contact pairs in GIDAS with the contact force transducer data of the FE collision simulation for case 1170986. The presented data of the PHBM was previously published [20].

Injury assessment

The results of injury predictions of the AHBM using the deterministic method (DM) and probabilistic method (PM) are summarised in Table V and are compared with the sustained injuries documented in the GIDAS cases. Further details are provided in the Appendix (Table A-I to Table A-III).

TABLE V

COMPARISON OF INJURIES REPORTED IN GIDAS AND PREDICTED BY THE ACTIVE HUMAN BODY MODEL.

		1050918			1170986			30090880		
			AHBM			AHBM			AHBM	
Body region		GIDAS	PM	DM	GIDAS	PM	DM	GIDAS	PM	DM
Head		TBI AIS2	AIS2+=51.2 % CSDM=0.25	-	TBI AIS2	AIS2+=85.2 % AIS3+=54.6 % CSDM=0.43	-	TBI AIS2	AIS1+=99.9 % AIS2+=32.5 % CSDM=0.18	-
Chest (rib fractures)		None	AIS1+=1.96 %	No	None	AIS1+=4.65 %	Yes	2	AIS1+=21.6 % AIS2+=1.7 %	Yes (1)
Pelvis		None	AIS2+=7.0 %	Yes	None	AIS2+=73.7 %	Yes	Bruise AIS1	AIS2+=82.6 %	Yes
Thigh	R	None	0.1 - 0.3 % (AIS3+)	Yes	None	0.0 – 0.1 % (AIS3+)	Yes	None	0.6 - 1.2 % (AIS3+)	Yes
	L	None	0.0 % (AIS3+)	Yes	None	0.1 - 0.2 % (AIS3+)	No	None	0.2 – 0.6 % (AIS3+)	Yes
Leg	R	None	0.0 – 0.9 % (AIS2+)	Yes	Graze (AIS1)	0.1 – 0.8 % (AIS2+)	No	None	0.3 - 0.8 % (AIS2+)	Yes
	L	Tibia, Fibula (AIS2)	0.8 – 8.1 % (AIS2+)	Yes	Bruise (AIS1)	0.8 – 14.8 (AIS2+)	Yes	None	0.8 – 46.3 % (AIS2+)	Yes

The results of the AHBM injury prediction are compared to the PHBM injury prediction, previously published [20], in Table VI. A detailed comparison is possible based on the details in the appendix of both studies (Table A-

I to Table A-III) and in A-Fig. 7 to A-Fig. 9 of this study. Results of the AHBM injury prediction for the *no collision simulation* are provided in Table A-IV and A-Fig. 10.

TABLE VI
COMPARISON OF PREDICTED INJURIES OF THE AHBM AND PHBM [20].

		1050918				1170986				30090880			
		AHBM		PHBM		AHBM		PHBM		AHBM		PHBM	
Body region		PM	DM	PM	DM	PM	DM	PM	DM	PM	DM	PM	DM
Head		AIS2+=51.2 % CSDM=0.25	-	AIS2+=72.9 % CSDM=0.35	-	AIS2+=85.2 % AIS3+=54.6 % CSDM=0.43	-	AIS2+=57.8 % CSDM=0.28	-	AIS1+=99.9 % AIS2+=32.5 % CSDM=0.18	-	AIS2+=80.2 % CSDM=0.39	-
Chest (rib fractures)		AIS1+=1.96 %	No	AIS1+=10.3 %	No	AIS1+=4.65 %	Yes	AIS1+=10.3 %	No	AIS1+=21.6 % AIS2+=1.7 %	Yes (1)	AIS1+=29.4 % AIS2+=2.46 %	Yes (1)
Pelvis		AIS2+=7.0 %	Yes	AIS2+=1.5 %	No	AIS2+=73.7 %	Yes	AIS2+=7.0 %	No	AIS2+=82.6 %	Yes	AIS2+=37.9 %	Yes
Thigh	R	0.1 - 0.3 % (AIS3+)	Yes	0.0 - 0.6 % (AIS3+)	Yes	0.0 – 0.1 % (AIS3+)	Yes	0.0 % (AIS3+)	Yes	0.6 - 1.2 % (AIS3+)	Yes	0.2 - 1.9 % (AIS3+)	Yes
	L	0.0 % (AIS3+)	Yes	0.0 % (AIS3+)	No	0.1 - 0.2 % (AIS3+)	No	0.0 - 0.6 % (AIS3+)	No	0.2 – 0.6 % (AIS3+)	Yes	0.3 – 0.9 % (AIS3+)	None
Leg	R	0.0 – 0.9 % (AIS2+)	Yes	0.1 - 1.3 % (AIS2+)	No	0.1 – 0.8 % (AIS2+)	No	0.0 - 2.1 % (AIS2+)	No	0.3 - 0.8 % (AIS2+)	Yes	0.6 - 2.6 % (AIS2+)	No
	L	0.8 – 8.1 % (AIS2+)	Yes	1.5 – 10.5 % (AIS2+)	Yes	0.8 – 14.8 (AIS2+)	Yes	1.2 – 9.4 (AIS2+)	Yes	0.8 – 46.3 % (AIS2+)	Yes	1.1 – 36.2 % (AIS2+)	Yes

IV. DISCUSSION

In the following subsections, the results of each GIDAS simulation pair will be discussed separately, followed by a summary for all cases. The results of the PHBM simulations, which are discussed below in comparison with the AHBM results and the GIDAS data, are available in a previously published study [20].

Case 1050918

Kinematics and collision points

Based on the comparison with the previously published PHBM results [20], visual evaluation of collision points (A-Fig. 4) shows nearly identical motion of the cyclist and locations of impact on the vehicle front end. At the time of head to windshield impact (275 ms), a slightly greater lateral rotation of the head to the left can be seen for the AHBM of this study. Further, the movement of the arms of the PHBM and AHBM was slightly different. Based on this minimal deviation, an identical match between simulation data with GIDAS can be stated regarding collision points for the PHBM and AHBM. The conclusion on identical kinematic behaviour is further supported by data on whole-body kinematics, shown in A-Fig. 1, for the entire simulation time.

Contact pairs

The contact force data of the PHBM and AHBM (A-Fig. 5) showed that the injury inducing contact pairs from GIDAS can be confirmed based on data of both HBMs. The maximum resultant force for both contact pairs ‘bumper to left leg’ (AHBM: 3.1 kN, PHBM: 3.5 kN) and ‘windshield to head’ (AHBM: 3.2 kN, PHBM: 3.8 kN) were lower for the AHBM and a rather gradual increase of contact force could be observed based on the curve shapes compared to the PHBM.

Injury assessment

Results from probabilistic and deterministic injury assessment of the AHBM is compared with GIDAS (Table V), and with the PHBM results (Table VI). Additional details are provided in the Appendix (Table A-I, A-Fig. 7). Regarding probabilistic injury assessment, a lower CSDM value resulted from the AHBM simulation, thus slightly lower abbreviated injury scale (AIS)2+ injury risk than for the PHBM simulation. Based on the previously defined threshold of 50 % [20] that an AIS-based injury risk must exceed, in order to be counted as match with the reported injuries from GIDAS, both AHBM (AIS2+=51.2 %) and PHBM (AIS2+= 72.9 %) matched the first degree (I°) traumatic brain injury (TBI) of AIS2 documented for this accident case in GIDAS. Further, this is in agreement with the previously described lower maximum resultant contact forces of head and windshield for the AHBM. The documented tibia and fibula fracture (AIS2) in the left leg from GIDAS were not predicted by both the AHBM

(AIS2+$_{max}$=8.1 %) and PHBM (AIS2+$_{max}$=10.5 %). For all other body regions (thorax, pelvis, thighs and right leg), the injury risks for the AHBM were either equal or lower than for the PHBM for this accident case. The pelvis injury risk for a 45 year old (YO), being the closest approach to the cyclist age of 32YO based on the available injury risk curves, depends on the quartile value of the MPS distribution (Q95 or Q99) selected as injury value for the injury risk prediction. The AHBM did not predict a pelvis fracture for both of the two quartile values, while the PHBM predicted a pelvis fracture only based on the Q99 injury value. Based on the deflection criterion, nearly identical low injury risk could be obtained for both AHBM (AIS2+=0.7 %) and the PHBM (AIS2+=0.5 %). The results of the pelvis deflection criterion better matched the GIDAS data, where no pelvis injury was reported, than the MPS data.

Results from deterministic injury prediction (Table A-I) showed that the MPS of specific body regions were higher for the AHBM than for the PHBM for the following body regions: lumbar spine, pelvis, right and left thigh, right knee, and right ankle. Exceptions, where the MPS were slightly lower for the AHBM, are the thorax (rib fractures), right and left tibia. For others, the MPS were found to be almost identical for both HBM, e.g., left knee and the feet. Therefore, it can be assumed that the muscle system implemented in the AHBM seems to directly influence at least specific elements in the respective body regions, where higher maximum MPS values were found. These maximum MPS values might result directly from the force acting on the specific cortical bone regions by attachment of the muscle elements and their predefined muscular activity. This assumption is further supported by the results of the *no collision simulation* for the respective body regions (Table A-IV, A-Fig. 10). Body regions of deterministic fracture prediction coincide with body regions of highest muscle injury risk (A-Fig. 11). For the PHBM, the deterministic fracture prediction for the right femur and patella most likely originated from a difference in bicycle geometry for all GIDAS cases, as described in a previous study [20]. The interaction of the distal femur region with the bicycle crossbar also occurred for the AHBM, but its effects were most likely masked by the effect of the muscle contraction on single element strains resulting in very high maximum MPS values, independent of the interaction with the bicycle. In general, the results from deterministic injury prediction need to be treated with caution, as individual differences in anatomy or response to loading are not considered. Further, the effect of muscle contraction-induced strain in cortical bone elements was only considered by the calculation method described in the method section for the probabilistic strain-based pelvis criterion, but not for the deterministic MPS calculation.

The trend of higher maximum MPS values from deterministic injury prediction in the abovementioned body regions was found for all numerically replicated GIDAS cases. Based on the results of the *no collision simulation*, it could be observed that the femoral head was being pulled towards the acetabulum leading to high strains in both the pelvis and femoral head region (Table A-IV, A-Fig. 10), and also for the respective muscle elements (A-Fig. 11). These results most likely originated from the different 'anatomy' of the multibody model used to calibrate the muscle model and the THUMS modelling approach of this body region, as previously described in detail in the method section. Additionally, the number of muscle elements is higher for the spine region than for the other body regions. Based on the previously described effect, that muscle contraction could directly influence few elements that contribute to the maximum MPS values (Table A-I), this would also explain the higher maximum MPS values in the lumbar spine. As this trend was found for all cases, it will not be further discussed in detail for *Case 1170986* and *30090880*.

Case 1170986

Kinematics and collision points

The collision points of the PHBM and AHBM (Fig. 4, A-Fig. 4) were almost identical. Regarding kinematics, a deviation can be seen for the final position of the upper and lower extremities of the AHBM and PHBM (Fig. 3, A-Fig. 2). For the AHBM a lateral rotation of the head to the left compared to the PHBM can be observed.

Contact pairs

Contact force data of the PHBM and AHBM (Fig. 5, A-Fig. 5) showed that the injury inducing contact pairs from GIDAS can be confirmed based on data of both HBMs. The maximum resultant forces for the AHBM simulation were lower for the contact pair 'hood to left leg' (AHBM: 1.6 kN, PHBM: 2.4 kN) and 'THUMS to bicycle' (AHBM: 4.8 kN, PHBM: 6.9 kN) and higher for the 'bumper to left leg' (AHBM: 4.5 kN, PHBM: 4.3 kN) and 'windshield to head' (AHBM: 4.2 kN, PHBM: 3.3 kN) compared to the PHBM.

Injury assessment

The difference in contact forces of the abovementioned contact pairs is in agreement with the probabilistic injury prediction when comparing both HBMs (Table V, Table VI, A-Fig. 8 and details for the AHBM in Table A-II). A higher CSDM value was calculated for the AHBM than for the PHBM simulation, resulting in higher brain injury risk for the AHBM (AIS2+=85.2 %, AIS3+=54.6 %) than for the PHBM (AIS2+=57.8 %). Thus, the TBI-I° reported in GIDAS was matched by the PHBM, but overpredicted by the AHBM. For the left and right leg, bruises and grazes are documented in GIDAS. The injury risk in the left leg was slightly higher for the AHBM ($AIS2+_{max}$=14.8 %) than for the PHBM ($AIS2+_{max}$=9.4 %), which is in agreement with the contact force data. In GIDAS, a bruise has been reported for the left leg. Based on contact force and injury data, for both HBMs there is chance of there being a bruise. However, the injury risk functions used in this study were not developed or validated for the prediction of minor injuries (AIS1), such as bruises or grazes. Therefore, prediction of these minor injuries is not possible based on probabilistic or deterministic injury criteria. The pelvis injury risk is much higher considering the MPS Q95 injury value for the AHBM ($AIS2+_{Q95}$=73.7 %) than for the PHBM ($AIS2+_{Q95}$=7.0 %); when considering the MPS Q99 injury value, the risk is lower for the AHBM ($AIS2+_{Q99}$=53.4 %) than for the PHBM ($AIS2+_{Q99}$=75.0 %). Based on the deflection criterion, nearly identical low injury risks were obtained for both the AHBM (AIS2+=0.4 %) and the PHBM (AIS2+=1.0 %). The results of the pelvic deflection criterion were more consistent with the GIDAS data, where no pelvic injuries were reported, than with the MPS data.

Results from deterministic injury assessment (Table A-II) shows similar trends as for *Case 1050918*. For the AHBM, the maximum MPS values were much higher than for the PHBM for the following body regions: lumbar spine, pelvis, right and left thigh, right knee, right fibula and right ankle. For other body regions, the values were either similar or slightly lower. A detailed discussion on the body regions with much higher maximum MPS is provided in the corresponding subsection of *Case 1050918*.

Case 30090880

Kinematics and collision points

The collisions points of the PHBM and AHBM (A-Fig. 4) were almost identical. Regarding kinematics, a larger deviation of the final positions of the AHBM and the PHBM can be seen (A-Fig. 3), than for the other cases. The THUMS is flying on and over the roof edge, where additional head contact occurred with the roof with a resultant contact force of 1.5 kN. For the PHBM, no further head collision occurred after the windshield collision.

Contact pairs

Contact force data of the PHBM and AHBM (A-Fig. 5) showed that the injury inducing contact pairs from GIDAS can be confirmed based on data of both HBMs. The maximum resultant forces for the AHBM simulation were lower for the contact pair ‘windshield to head’ (AHBM: 2.9 kN, PHBM: 3.1 kN) and higher for ‘hood to buttock’ (AHBM: 0.6 kN, PHBM: 0.5 kN), ‘hood to torso’ (AHBM: 1.2 kN, PHBM: 1.0 kN) and ‘windshield to torso’ (AHBM: 1.6 kN, PHBM: 1.4 kN) compared to the PHBM. Additionally, the abovementioned contact ‘roof to windshield’ occurred for the AHBM with a maximum resultant force of 1.5 kN, as well as a ‘bumper to left leg’ (AHBM: 5.6 kN, PHBM: 5.5 kN) contact for both HBMs, where no injury inducing contact pair was reported in GIDAS.

Injury assessment

The difference in contact forces of the abovementioned contact pairs is in agreement with the probabilistic injury prediction when comparing both HBMs (Table V, Table VI, A-Fig. 9 and details for the AHBM in Table A-III). A lower CSDM value was calculated for the AHBM than for the PHBM simulation, resulting in a lower brain injury risk for the AHBM (AIS1+= 99.9 %, AIS2+=32.5 %) than for the PHBM (AIS2+=80.2 %, AIS3+=48.8 %). Thus, the TBI-I° reported in GIDAS was matched by the PHBM, but underpredicted by the AHBM. The two fractured ribs were underpredicted based on the rib fracture prediction by both the AHBM (AIS1+=21.6 %) and the PHBM (AIS1+=29.4 %). Based on the GIDAS documentation, the thorax collision might have occurred in the region of the windshield wipers (A-Fig. 4), which were not part of the FE car model. As the windshield wipers can be slightly stiffer than the surrounding windshield and hood, a collision of the thorax with the windshield wipers can lead to a peak punctual load placed on individual ribs. The lack of windshield wipers in the FE model might therefore be the reason for the underpredicted risk of rib fracture, despite the agreement of the thorax collision point (A-Fig. 4) [20]. The 56YO cyclist sustained a bruise on the pelvis (AIS1), that cannot be directly compared with the

probabilistic (AIS2+) and deterministic injury prediction for this body region. However, the PHBM MPS Q95 results matched the reported injury better than the MPS Q99 and AHBM predictions. The pelvis injury risk (45YO – 65YO, as the victim age was 56YO) is much higher considering the MPS Q95 injury value for the AHBM ($AIS2+_{Q95}$=68.2 – 82.6 %) than for the PHBM ($AIS2+_{Q95}$=22.0 – 37.9 %); when considering the MPS Q99 injury value, the risk is lower for the AHBM ($AIS2+_{Q99}$=45.9 – 61.4 %) than for the PHBM ($AIS2+_{Q99}$=88.5 – 94.4 %). Based on the deflection criterion, a nearly identical low injury risk could be obtained for both the AHBM (AIS2+=0.3 %) and the PHBM (AIS2+=1.0 %), which can be assumed to have underpredicted the sustained bruise (AIS1). No injury was reported for the lower extremities in GIDAS and neither HBM exceeded the selected threshold of 50 % regarding lower extremity injury risk (AIS2+). However, a bruise or graze (AIS1) could be expected based on the injury prediction of the AHBM ($AIS2+_{max}$=46.3 %) and the PHBM ($AIS2+_{max}$=36.2 %). After consultation with GIDAS accident research specialists, an underrepresentation of less critical injuries, such as tibia bruises or fractures, can in general be assumed if more severe injuries, e.g., head or chest, are present. As there was much less documentation available on case 30090880 compared to the other cases, a lack of detailed information on this GIDAS accident can be assumed, resulting in possibly missing information on, e.g. tibia or fibula hairline fractures or full fractures [20].

Results from deterministic injury assessment (Table A-II) shows similar trends as for *Case 1050918*. For the AHBM the maximum MPS values were much higher than for the PHBM for the following body regions: lumbar spine, pelvis, left thigh, right knee, and right fibula. For the other body regions, the values were either similar or slightly lower. A detailed discussion on the body regions with much higher maximum MPS is provided in the corresponding subsection of *Case 1050918*.

General

For all GIDAS cases, collision simulation data of the AHBM matched the corresponding GIDAS documentation equally well regarding collision points and contact pairs. Based on the selected threshold of 50 %, the AIS-based injury risk predictions were compared to the sustained injuries with the same AIS level reported in GIDAS. For *Case 1050918*, the AHBM and PHBM injury risk prediction matched the reported injuries in GIDAS equally well. For *Case 1170986*, the AHBM overpredicted the CSDM-based brain injury risk and the PHBM prediction matched the reported TBI I° (AIS2) injury. For *Case 30090880*, the AHBM underpredicted the CSDM-based brain injury risk while the PHBM matched the reported TBI I° (AIS2) injury. Based on these results and the detailed description regarding the pelvis-femur interaction due to muscular contraction and the modelled gap in this body region in the THUMS in the corresponding subsection of *Case 1050918*, it can be assumed that an HBM must be modelled in a way that allows for a contracting muscle system to be implemented in the first place. Otherwise, the implementation of a muscle system will lead to unphysiologically high strains even without an impact occurring, although it brings the HBM closer to the stabilising or reaction behaviour of a human. The THUMS used in this study had not been developed for the implementation of a muscle system, but future AHBM approaches in VRU safety research should consider this aspect. Regarding probabilistic injury assessment of the pelvis, the presented approach to calculate the injury values in a way that accounts for the abovementioned effect, would at least improve the injury prediction for the AHBM, but may not always lead to a better match with GIDAS compared to the PHBM. The forces on the hip created by the musculature far exceeded the loading caused by gravitational forces [54], hence the bone structures of PHBMs are not required to withstand the same stresses as in AHBMs.

An alternative might be to run a prior simulation step, probably for several seconds until the AHBM reaches the equilibrium point. Additional strains could be neglected by exporting the model without initial strains after this additional simulation step, comparable to a prior positioning simulation step for HBM. Thus, the initial muscle contraction during the collision simulation might affect the pelvis injury prediction less than in the simulations presented in this study. However, an additional simulation step might lead to a different initial position for the collision simulations of the AHBM compared to the PHBM, which might influence the comparability of the two models. Due to time and resource constraints, an additional simulation step and a detailed comparison with the AHBM results presented was not possible in this study. However, a more detailed analysis of this approach would be interesting for future studies to investigate ways to include a contracting muscle system in an FE HBM that had not been particularly developed for such implementation. Other AHBM approaches encountered similar challenges when implementing activatable muscles in PHBM, that are based on the PHBM modelling approach. For example, elbow joint deformations [55] and knee joint deformations [56] were affected in previous studies. This further supports our assumption, that the HBM must be modelled in a way to allow for physiological

implementation of activatable muscles in the first place.

By comparison of the AHBM and PHBM, the following trends could be found regarding injury risk prediction. For *Case 1050918*, the injury risk was mostly reduced by the implementation of the muscle system, for *Case 1170986*, the injury risk increased for the brain, slightly increased for the lower legs and slightly decreased for the thorax, and for *Case 30090880*, the injury risk shifted from the head to the lower extremities by the implementation of the muscle system. For the head, the CSDM prediction better matched the AIS2 TBI of GIDAS especially for the PBHM, while the brain injury criterion (BrIC) injury risk overpredicted the sustained injuries in all cases for both the AHBM and PHBM. No pelvis fracture was reported in GIDAS for any of the cases, only a bruise (AIS1) was reported for *Case 30090880*. Based on this data, the AIS2+ pelvis deflection-based injury risk (≤1 % for both the AHBM and the PHBM) better matched the GIDAS data. However, based on the GIDAS documentation, a significant increase in pelvis deflection-based injury risk would be expected for *Case 30090880*, which is not the case. For the strain-based pelvis injury criterion, the PHBM showed a better match with GIDAS regarding MPS Q95 based injury risk prediction, while for the AHBM, the MPS Q99 performed better for two out of three cases in comparison with GIDAS. The partly counterintuitive development of the MPS-based quartile values for the AHBM, i.e., for case 1170986, is a possible consequence of the adapted calculation method described in the methods section. Depending on the time-dependent development of the MPS in the *no collision simulation* compared to the *collision simulation*, the final MPS Q95 value considered for injury risk prediction can result in a smaller difference than for the MPS Q99 value, thus leading to higher values for MPS Q95 than for MPS Q99. For the PHBM [20], the MPS Q95 values are always smaller than the MPS Q99 values, as they are obtained directly from maximum MPS distribution as further described in the literature [52].

In the selected cases, the most frequent injuries of the injury distribution extracted from comparable GIDAS accident data [20] are covered, except for upper extremity injuries. This general tendency could be covered by both the AHBM and PHBM simulations. As described in further detail in our previous study [20], the type of accident [57] and most common injury inducing contact pairs [58] matches both for GIDAS and the PHBM and AHBM predictions. As no reliable injury criterion for upper extremities is currently available to the best knowledge of the authors, and because no upper extremity injuries were reported in the selected GIDAS cases, this body region was not considered for probabilistic and deterministic injury assessment in this study, but might be of interest in the future. Regarding the correlation of injury risks with collision velocity and VRU age [59], data from GIDAS, AHBM and PHBM, partially matches this trend. However, based on the small sample size of accident cases, a profound confirmation of these trends is not possible and is therefore not further discussed at this point.

To be able to compare AHBM and PHBM results, the authors were restricted regarding FE bicycle model selection and further adaption to possibly better match the individual bicycles of each GIDAS case. An averaged bicycle based on GIDAS accident data have previously been developed [20] and applied accordingly in this study. A similar approach was taken in the NCAP CATS project [60], where a mean bicycle and cyclist based on European data were developed and applied. Due to time and resource constraints, not every aspect of the single GIDAS cases could be replicated in detail in the FE simulation. Nevertheless, it would be an interesting aspect to investigate the effect of replicating each accident case more closely, i.e., regarding the bicycle model, different pedal positions, morphing the HBM to the anthropometry of the accident victim or to develop a detailed FE model of each car involved in the GIDAS cases, rather than using the same car model for each GIDAS case.

In this study, car-to-cyclist collisions were analysed with an initial car velocity at the time of collision ranging from 30 km/h to 47 km/h. For this range, the PHBM performed better than the AHBM. In low speed cases with relative velocities of less than 30 km/h, the stabilising effect of musculature might be even more important. For such cases, it is less likely that moderate (AIS2) or higher injuries would occur. Therefore, the comparison of sustained injuries in low speed GIDAS cases with the presented whole-body injury prediction of the HBM would be limited by the prediction capabilities regarding minor injuries (AIS1) of the AHBM and PHBM based on the available injury criteria. In addition, muscle or tendon injuries are hardly reported in GIDAS nor are long-term injuries that might be comparable to muscle injury prediction presented in this study. Future research in this field would benefit from reliable HBM-applicable injury criteria for minor injuries (AIS1), as well as from a more detailed documentation in GIDAS of minor injuries and long-term muscle and tendon injuries in accident victims.

V. CONCLUSIONS

In this study, we developed and implemented a muscle system into the THUMS and used the resulting AHBM in a previously developed simulation setup to compare the results with GIDAS accident data. In addition, the previously published PHBM results were compared with the AHBM results of this study. Kinematics, collision points and injury inducing contact pairs matched very well for both PHBM and AHBM. For *Case 1050918* the AHBM and PHBM injury risk prediction matched the reported injuries in GIDAS equally well, for *Case 1170986* the AHBM overpredicted the CSDM-based brain injury risk and the PHBM prediction matched the reported TBI I° (AIS2) injury, and for *Case 30090880* the AHBM underpredicted the CSDM-based brain injury risk, while the PHBM matched the reported TBI I° (AIS2) injury. From the data presented, it can be concluded that the PHBM and AHBM predictions are in equally good agreement with the available data of the selected accident cases. Especially with regard to probabilistic injury assessment, the PHBM predictions are in better agreement with the data on sustained injuries of the selected accident cases than the AHBM predictions. Based on the data from pelvis injury risk prediction and deterministic injury prediction, it can be assumed that future HBM developments should consider a possible implementation of muscle systems in the early stages of the model development. When implementing a muscle system into an already existing HBM, an additional simulation step to calculate an equilibrium point prior to the collision simulation could improve the AHBM prediction in comparison to GIDAS, but would also introduce new uncertainties such as a resulting difference in final posture compared to the PHBM. A possible future goal would be to bring the FE models even closer to their real-life counterpart, which could include a closer approximation of the actual bicycle, car and VRU involved in the accident case.

VI. ACKNOWLEDGEMENT

This work was supported by the Federal Ministry for Economic Affairs and Climate Action of Germany (Bundesministerium für Wirtschaft und Klimaschutz) through the project *Artificial Intelligence for Real-Time Injury Prediction (ATTENTION)*, Grant Number 19A21027D. Further, the authors would like to thank Christian Kleinbach (Mercedes-Benz AG, Germany) and Dirk Freßmann (DYNAmore GmbH, an Ansys Company, Germany), as well as Niranjan Ballal, Thomas Soot, Patrick Matt, Marcin Jenerowicz and Matthias Boljen (Fraunhofer EMI, Germany) for their contributions in the ATTENTION project, including contributions to the work presented in this study.

VII. AUTHOR'S CONTRIBUTIONS

The authors declare no conflict of interest. The authors contributed to this manuscript as follows:

Niclas Trube was involved regarding conceptualisation, methodology, writing – original draft, visualisation and funding acquisition. This involved the development of a methodology to reconstruct GIDAS accidents as FE collision simulations in LS-DYNA. Regarding the results presented in this work, he mainly contributed to the extraction, evaluation and visualisation of data from the AHBM collision simulations that were relevant for the comparison with GIDAS accident data and the previously published PHBM results.

Patrick Lerge participated in the development of the methodology and the writing of the original draft. This includes in particular the development of both the MB ABHM and the FE ABHM, the programme development for the model transfer, the execution of the multibody pre-simulations, as well as the provision of the repositioning target files for the OASYS Primer based repositioning of the THUMS v4.02 pedestrian into the described cyclist posture.

Lennart V. Nölle participated in the writing of the original draft and performed the muscle strain injury analysis, including all computational steps and visualisations associated with the strain injury assessment.

Jörg Mönnich was particularly involved in the analysis of GIDAS data and extracted necessary information from the GIDAS datasets. Using information from real accidents (GIDAS), the FEM simulations were made plausible or supplemented with input parameters through further accident reconstruction.

Thomas Lich was involved regarding the reviewing and proofreading of the publication. Specifically, he cross-checked the accuracy of the sample accidents from GIDAS and compared the results obtained from the FE simulation with those of the GIDAS real accidents to provide a subjective assessment of the simulation's quality. Finally, additional topics for the discussion and conclusion section was provided.

Syn Schmitt was involved in the conceptualisation, methodology, resources, writing - review and editing, supervision, and funding acquisition.

VIII. REFERENCES

[1] Slootmans, F. (2021) Vias institute, *European Road Safety Observatory. Facts and Figures - Cyclists - 2021*.

[2] Statistisches Bundesamt (Destatis). (2021) *Verkehrsunfälle - Kraftrad- und Fahrradunfälle im Straßenverkehr 2020*, Wiesbaden (Germany).

[3] Adminaité-Fodor, D.; Jost, G. (2020) *How safe is walking and cycling in Europe? Pin Flash Report 38*, Brussels (Belgium).

[4] Katsuhara, T.; Miyazaki, H.; Kitagawa, Y.; Yasuki, T. (2014) Impact kinematics of cyclist and head injury mechanism in car-to-bicycle collision. *Proceedings of the IRCOBI Conference*, 2014, Berlin (Germany).

[5] Pipkorn, B. (2021) State-of-the-Art Human Body Modelling (HBM) Analysis for Cyclist Airbags, 2021, Virtual conference.

[6] Leo, C.; Gruber, M.; Feist, F.; Sinz, W.; Roth, F.; Klug, C. (2020) The Effect of Autonomous Emergency Braking Systems on Head Impact Conditions for Pedestrian and Cyclists in Passenger Car Collisions. *Proceedings of the IRCOBI Conference*, 2020, Munich (Germany).

[7] Klug, C.; Feist, F.; Wimmer, P. (2018) Simulation of a Selected Real World Car to Bicyclist Accident using a Detailed Human Body Model. *Proceedings of the IRCOBI Conference*, 2018, Athen (Greece).

[8] N. Bourdet; C. Deck; T. Serre; C. Perrin; M. Llari; R. Willinger. (2014) In-depth real-world bicycle accident reconstructions. International Journal of Crashworthiness, **19**(3): 222–232.

[9] Shigeta, K.; Kitagawa, Y.; Yasuki, T. (2009) Development of Next Generation Human FE Model capable of Organ Injury Prediction. *Proceedings of the 21st Annual Enhanced Safety of Vehicles*, 2009, Stuttgart (Germany).

[10] Untaroiu, C. D.; Pak, W.; Meng, Y.; Schap, J.; Koya, B.; Gayzik, S. (2017) A Finite Element Model of a Midsize Male for Simulating Pedestrian Accidents. Journal of Biomechanical Engineering, **140**(1).

[11] John, J.; Klug, C.; Kranjec, M.; Svenning, E.; Iraeus, J. (2022) Hello, world! VIVA+: A human body model lineup to evaluate sex-differences in crash protection. Frontiers in bioengineering and biotechnology, **10**(918904).

[12] Toyota Motor Corporation, Toyota Central R&D Labs., Inc. (2021) *Documentation Total Human Model for Safety (THUMS) AM50 Pedestrian Model Version 4.02*.

[13] Wu, T.; Kim, T. et al. (2017) Evaluation of biofidelity of THUMS pedestrian model under a whole-body impact conditions with a generic sedan buck. Traffic injury prevention, **18**(sup1): S148-S154.

[14] Forman, J. L.; Joodaki, H. et al. (2015) Whole-body Response for Pedestrian Impact with a Generic Sedan Buck. Stapp Car Crash Journal, **59**: 401–444.

[15] Forman, J. L.; Joodaki, H. et al. (2015) Biofidelity Corridors for Whole-Body Pedestrian Impact with a Generic Buck. *Proceedings of the IRCOBI Conference*, 2015, Lyon (France).

[16] Konikow, L. F.; Bredehoeft, J. D. (1992) Ground-water models cannot be validated. Advances in Water Resources, **15**(1): 75–83.

[17] Oreskes, N.; Shrader-Frechette, K.; Belitz, K. (1994) Verification, validation, and confirmation of numerical models in the Earth sciences. Science, **263**(5147): 641–646.

[18] Lund, M. E.; Zee, M. de; Andersen, M. S.; Rasmussen, J. (2012) On validation of multibody musculoskeletal models. Proceedings of the Institution of Mechanical Engineers. Part H, Journal of engineering in medicine, **226**(2): 82–94.

[19] Hammer, M. (2024) University of Stuttgart, *Biophysical validity of reduced soft-tissue modelling in neuro-musculoskeletal simulations (PhD thesis)*, Stuttgart (Germany).

[20] Trube, N.; Matt, P. et al. (2023) Plausibility Assessment of Numerical Cyclist to Vehicle Collision Simulations based on Accident Data. *Proceedings of the IRCOBI Conference*, 2023, Cambridge (UK).

[21] Lich, T.; Moennich, J.; and Schmidt, D.; Voss, M. (2022) Preparation of an AI based real-time injury risk index estimation by deriving road user behavior from video-documented crashes. *15th International Symposium and Exhibition on Sophisticated Car Safety System (airbag2022)*, 2022, Mannheim (Germany).

[22] Lich, T.; Mönnich, J.; Voss, M.; Lerge, P.; Nölle, L. V.; Schmitt, S. (2023) Applying AI Methods On Video Documented Car-VRU Front Crashes to Determine Generalized Vulnerable Road User Behaviors. *Proceedings of the 27th International Technical Conference on the Enhanced Safety of Vehicles (ESV)*, 2023, Yokohama (Japan).

[23] Iwamoto, M.; Nakahira, Y. (2015) Development and Validation of the Total HUman Model for Safety (THUMS) Version 5 Containing Multiple 1D Muscles for Estimating Occupant Motions with Muscle Activation During Side Impacts. Stapp Car Crash Journal, **59**: 53–90.

[24] Iwamoto M, N. Y. (2014) A Preliminary Study to Investigate Muscular Effects for Pedestrian Kinematics and Injuries Using Active THUMS. *Proceedings of the IRCOBI Conference*, 2014, Berlin (Germany).

[25] Lerge, P.; Schmitt, S.; Martynenko, O. V. (2020) Simulation of Pedestrian Kinematics before Impact with a Vehicle using an Active Pedestrian Human Body Model. *Proceedings of the IRCOBI Conference*, 2020, Munich (Germany).

[26] Lalwala, M.; Devane, K. S. et al. (2023) Development and Validation of an Active Muscle Simplified Finite Element Human Body Model in a Standing Posture. Annals of Biomedical Engineering, **51**(3): 632–641.

[27] Meijer, R.; van Hassel, E.; Broos, J.; Elrofai, H.; van Rooij, L.; van Hooijdonk, P. (2012) Development of a Multi-Body Human Model that Predicts Active and Passive Human Behaviour. *Proceedings of the IRCOBI Conference*, 2012, Dublin (Ireland).

[28] Günther, M.; Schmitt, S.; Wank, V. (2007) High-frequency oscillations as a consequence of neglected serial damping in Hill-type muscle models. Biological cybernetics, **97**(1): 63–79.

[29] Haeufle, D. F. B.; Günther, M.; Bayer, A.; Schmitt, S. (2014) Hill-type muscle model with serial damping and eccentric force-velocity relation. Journal of Biomechanics, **47**(6): 1531–1536.

[30] Kleinbach, C.; Martynenko, O.; Promies, J.; Haeufle, D. F. B.; Fehr, J.; Schmitt, S. (2017) Implementation and validation of the extended Hill-type muscle model with robust routing capabilities in LS-DYNA for active human body models. BioMedical Engineering OnLine, **16**(1): 109.

[31] Wochner, I.; Nölle, L. V.; Martynenko, O. V.; Schmitt, S. (2022) 'Falling heads': investigating reflexive responses to head-neck perturbations. BioMedical Engineering OnLine, **21**(1): 25.

[32] Martynenko, O. V.; Kempter, F. et al. (2023) Development and verification of a physiologically motivated internal controller for the open-source extended Hill-type muscle model in LS-DYNA. Biomechanics and Modeling in Mechanobiology, **22**(6): 2003–2032.

[33] Klein Horsman, M. D.; Koopman, H. F. J. M.; van der Helm, F. C. T.; Prosé, L. P.; Veeger, H. E. J. (2007) Morphological muscle and joint parameters for musculoskeletal modelling of the lower extremity. Clinical Biomechanics, **22**(2): 239–247.

[34] Arnold, E. M.; Ward, S. R.; Lieber, R. L.; Delp, S. L. (2010) A model of the lower limb for analysis of human movement. Annals of Biomedical Engineering, **38**(2): 269–279.

[35] Driess, D.; Zimmermann, H. et al. (2018) Learning to Control Redundant Musculoskeletal Systems with Neural Networks and SQP: Exploiting Muscle Properties. *IEEE International Conference on Robotics and Automation (ICRA)*.

[36] Meszaros-Beller, L.; Hammer, M.; Riede, J. M.; Pivonka, P.; Little, J. P.; Schmitt, S. (2023) Effects of geometric individualisation of a human spine model on load sharing: neuro-musculoskeletal simulation reveals significant differences in ligament and muscle contribution. Biomechanics and Modeling in Mechanobiology, **22**(2): 669–694.

[37] Schmitt, S. (2022) *demoa-base: a biophysics simulator for muscle-driven motion*.

[38] Walter, J. R.; Günther, M.; Haeufle, D. F. B.; Schmitt, S. (2021) A geometry- and muscle-based control

architecture for synthesising biological movement. Biological Cybernetics, **115**(1): 7–37.

[39] German in-depth accident study (GIDAS) – www.gidas.org. Accessed and analysed by Bosch Accident Research, data weighted and representative for Germany (Data 2001 – 2022). [March 2024].

[40] Liers, H. (2018) Traffic accident research in Germany and the German in-depth accident study (GIDAS). *Society of Indian Automotive Manufactures (SIAM) Conference*, 2018.

[41] Ballal, N.; Soot, T.; Dlugosch, M.; Trube, N.; Fressmann, D. (2023) A method for efficient generation and optimization of simulation-based training data for data-driven injury prediction in vru-vehicle accident scenarios. *Proceedings of the 27th International Technical Conference on the Enhanced Safety of Vehicles (ESV)*, 2023, Yokohama (Japan).

[42] Center for Collision Safety and Analysis at the George Mason University (GMU), Federal Highway Administration (FHWA). "Toyota Camry Detailed Finite Element Model", Available: https://www.ccsa.gmu.edu/models/2012-toyota-camry. [March 2024].

[43] Hatze, H. (1977) A myocybernetic control model of skeletal muscle. Biological cybernetics, **25**(2): 103–119.

[44] Rockenfeller, R.; Günther, M. (2018) Inter-filament spacing mediates calcium binding to troponin: A simple geometric-mechanistic model explains the shift of force-length maxima with muscle activation. Journal of Theoretical Biology, **454**: 240–252.

[45] The MathWorks Inc. (2021) *MATLAB version: 9.10.0 (R2021a)*, Natick, Massachusetts, United States.

[46] Oasys Ltd. (2023) *PRIMER Version 20.1*.

[47] Chr. Ryf; A. Weymann. (1995) The neutral zero method — A principle of measuring joint function. Injury, **26**: 1–11.

[48] Nölle, L.; Lerge, P. et al. (2022) *EHTM Code and Manual*, Stuttgart (Germany).

[49] Lerge, P.; Trube, N.; Schmitt, S. "Replication Data for: "Development and plausibility assessment of an active human body model in numerical cyclist to vehicle collision simulations based on real-life accident data", DaRUS, V1. https://doi.org/10.18419/darus-4221. [June 2024].

[50] Nölle, L. V.; Mishra, A.; Martynenko, O. V.; Schmitt, S. (2022) Evaluation of muscle strain injury severity in active human body models. Journal of the mechanical behavior of biomedical materials, **135**: 105463.

[51] Garrett, W. E.; Safran, M. R.; Seaber, A. V.; Glisson, R. R.; Ribbeck, B. M. (1987) Biomechanical comparison of stimulated and nonstimulated skeletal muscle pulled to failure. The American Journal of Sports Medicine, **15**(5): 448–454.

[52] Peres, J.; Auer, S.; Praxl, N. (2016) Development and comparison of different injury risk functions predicting pelvic fractures in side impact for a Human Body Model. *Proceedings of the IRCOBI Conference*, 2016, Malaga (Spain).

[53] Klug, C.; Ellway, J. (2021) *Pedestrian Human Model Certification. Technical Bulletin TB024 Version 3.0.1*.

[54] Radin, E. L. (1980) Biomechanics of the human hip. Clinical orthopaedics and related research, (152): 28–34.

[55] Nölle, L. V.; Wochner, I.; Hammer, M.; Schmitt, S. (2024) Using muscle-tendon load limits to assess unphysiological musculoskeletal model deformation and Hill-type muscle parameter choice. bioRxiv.

[56] Jani, D.; Chawla, A.; Mukherjee, S.; Goyal, R.; Nataraju, V. (2009) Repositioning the Human Body Lower Extremity FE Model. SAE International Journal of Passenger Cars - Mechanical Systems, **2**(1): 1024–1030.

[57] Fredriksson, R.; Fredriksson, K.; Strandroth, J. (2014) Pre-crash motion and conditions of bicyclist-to-car crashes in Sweden. *Proceedings of the International Cycling Safety Conference*, 2014, Göteborg (Sweden).

[58] Hamacher, M.; Kühn, M.; Hummel, T. (2016) *Analyse der Radfahrer-Pkw-Kollision*, 65. *Gesamtverband der Deutschen Versicherungswirtschaft e.V. Unfallforschung der Versicherer*, Berlin (Germany).

[59] Moennich, J.; Lich, T.; Georgi, Andreas, Reiter, Nora. (2015) *Did a higher distribution of pedelecs results in more severe accidents in Germany?*, Stuttgart (Germany).

[60] Camp, O. O. den; van Montfort, S.; Uittenbogaard, J. (2016) Integrated vehicle safety, *CATS Deliverable 6.1: CATS Final project summary report. TNO report*, Helmond (Netherlands).

[61] Kerrigan, J. R.; Drinkwater, D. C.; Kam, C. Y.; Murphy, D. B.; Ivarsson. (2004) Tolerance of the human leg and thigh in dynamic latero-medial bending. International Journal of Crashworthiness, **9**(6): 607–623.

[62] Kuppa, S.; Wang, J.; Haffner, M.; Eppinger, R. (2001) Lower extremity injuries and associated injury criteria. SAE Technical Paper,

I. APPENDIX

The whole-body kinematics of each simulation is shown over time for each case in A-Fig. 1 to A-Fig. 3.

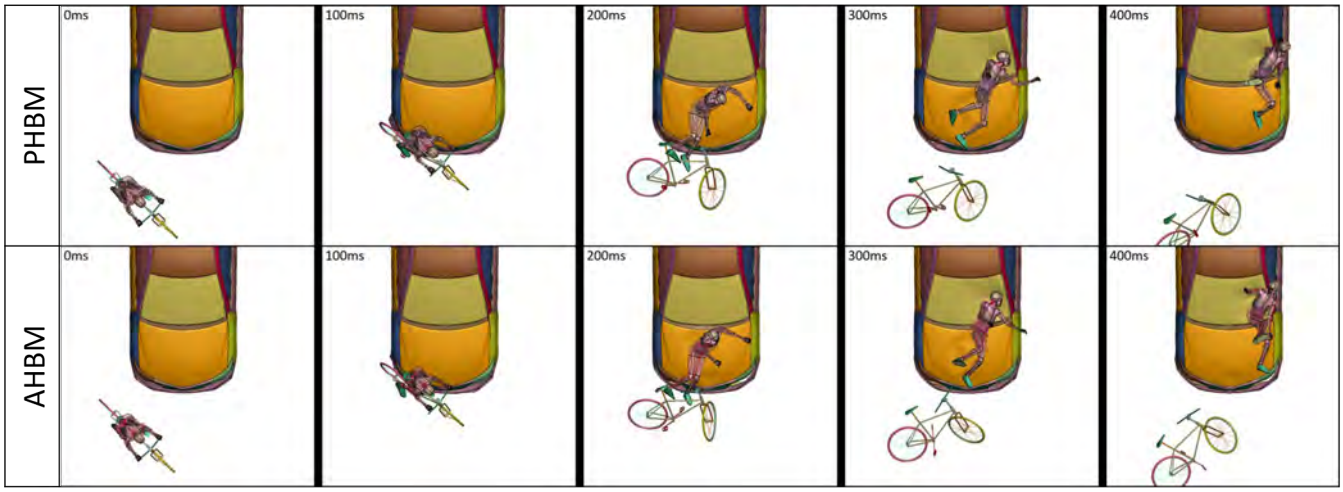

A-Fig. 1. Whole-body kinematics of the FE collision simulation for case 1050918. The presented data of the PHBM was previously published [20].

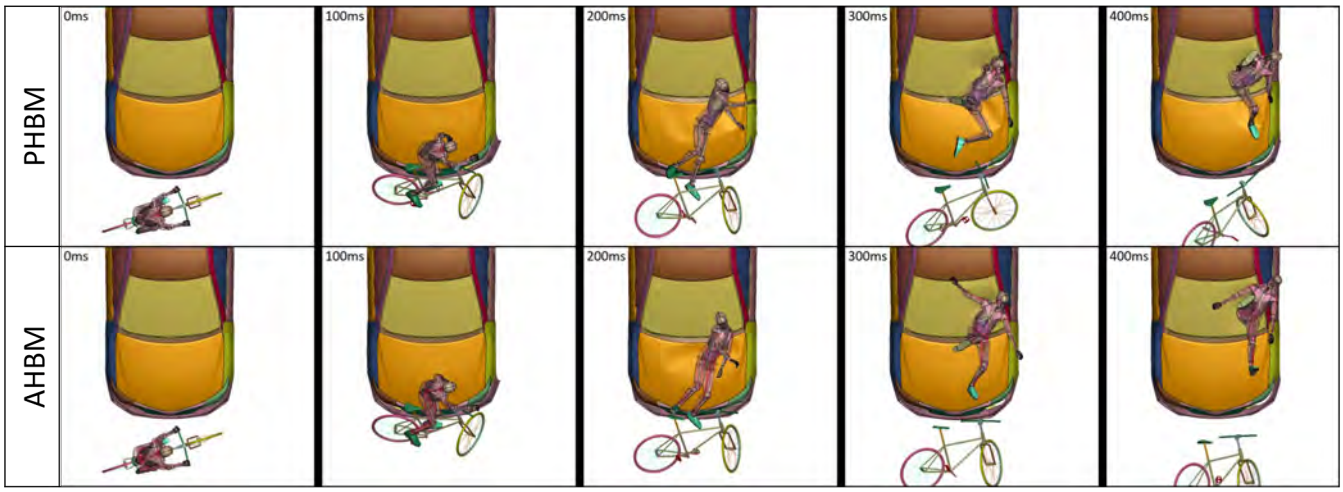

A-Fig. 2. Whole-body kinematics of the FE collision simulation for case 1170986. The presented data of the PHBM was previously published [20].

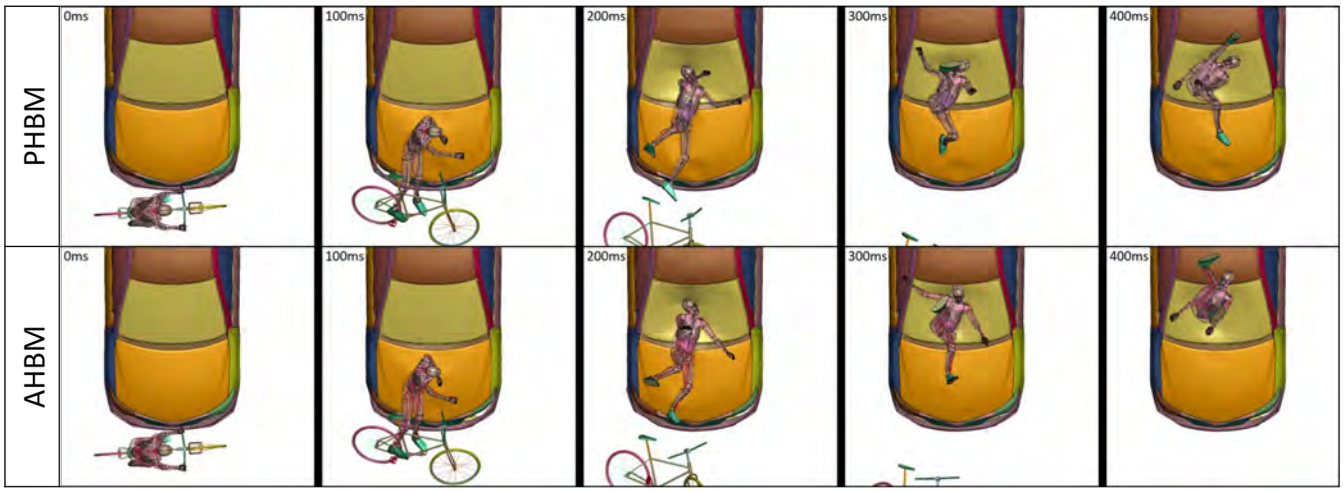

A-Fig. 3. Whole-body kinematics of the FE collision simulation for case 30090880. The presented data of the PHBM was previously published [20].

In A-Fig. 4, the comparison of individual collision points of specific body parts with vehicle components between GIDAS and the FE simulation is shown.

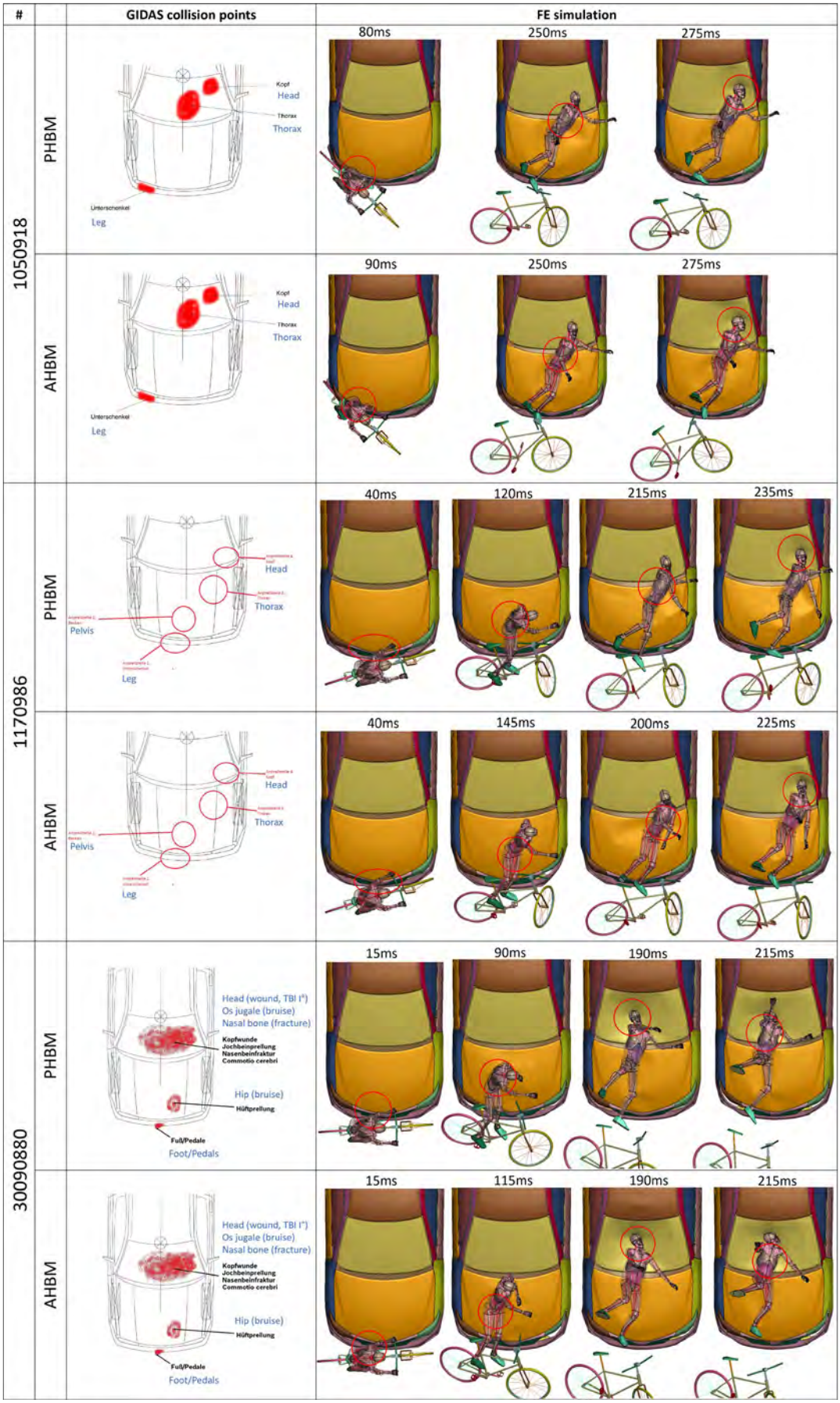

A-Fig. 4. Collision points of the cyclist and the vehicle in accident data and in the collision simulations regarding the documented body regions. English translations were added in blue based on the original image file from GIDAS. The presented data of the PHBM was previously published [20].

In A-Fig. 5, the documented injury-inducing GIDAS contact pairs and the corresponding resultant force data from the simulations are compared for each accident case. For each individual injury, a vehicle component was assigned as the primary contact partner in the GIDAS documentation.

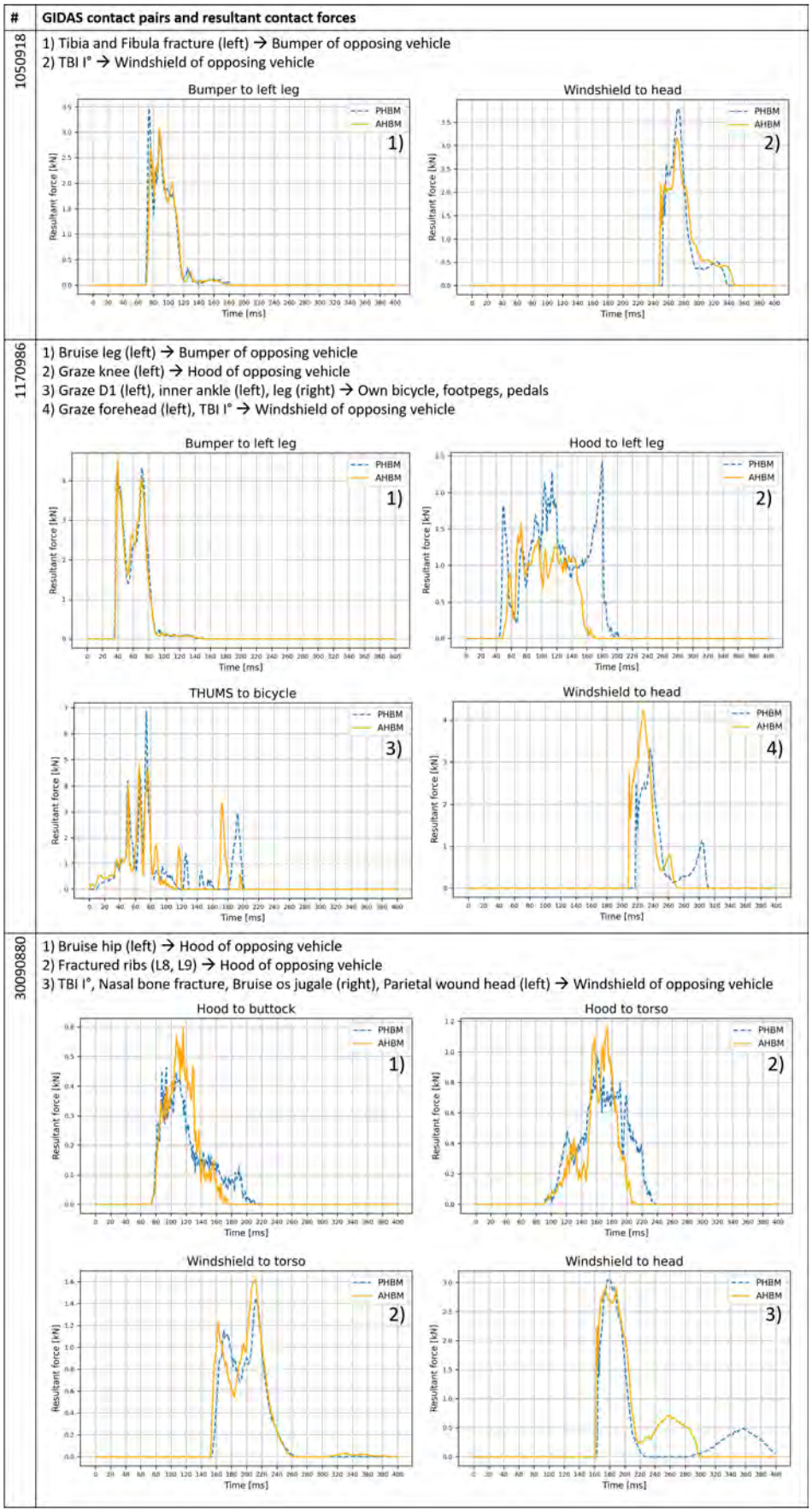

A-Fig. 5. Contact pairs in GIDAS compared with resultant contact forces between the THUMS body parts and vehicle components. The presented data of the PHBM has been previously published [20].

In A-Fig. 6 a previously published comparison between the bicycle FE model and the three bicycles of the GIDAS cases is shown.

FE model	1050918	1170986	30090880
			

A-Fig. 6. Comparison of the bicycle FE model and the bicycles of each GIDAS case [20].

In Table A-I to Table A-III and A-Fig. 7 to A-Fig. 9, details regarding sustained injuries (GIDAS) and predicted injuries (HBM) are presented. Results of the AHBM injury prediction for the *no collision simulation* are provided in Table A-IV and A-Fig. 10. Regarding deterministic injury prediction, the following bones were considered if multiple bones were relevant for a body region. For the ribs, all left and right ribs were considered with one maximum MPS value per rib. Based on this data, the maximum values as well as the 2nd and 3rd highest values of all ribs were calculated. For the lumbar spine, the L1 to L5 were considered. For the pelvis, the sacrum and all hip bones were considered. For the ankle, the talus and calcaneus were considered. For the foot, all cortical bones in the foot (except talus and calcaneus) were considered. For the other bones, individual cortical bone data could be used, e.g., right femur. Data on cortical bones are listed, for which an injury was documented in at least one of the three GIDAS cases. Grazes and bruises are generally documented as AIS1 injuries in GIDAS. For the evaluation of the probabilistic femur and tibia fracture criteria, the resultant moment ($M_{Resultant}$) [61] and the Revised Tibia Index (RTI) [62] were applied. The abovementioned information is consistent with the previously published data of the PHBM [20].

TABLE A-I

SUSTAINED INJURIES AND AHBM PREDICTIONS FOR GIDAS CASE 1050918

GIDAS		Probabilistic prediction			Deterministic prediction		
Region	Injury	Injury criterion	Injury value	Injury risk	Region	Max MPS	Threshold
Head	Traumatic brain injury I° (TBS, AIS2)	CSDM	0.25	AIS1+=100 % AIS2+=51.2 % AIS3+=25.6 % AIS4+=18.6 % AIS5+=17.5 %	-	-	-
	Head laceration (AIS1)	BrIC	1.28	AIS1+=100 % AIS2+=100 % AIS3+=87.6 % AIS4+=69.5 % AIS5+=65.5 %			
Thorax	-	Forman		AIS1+=1.96 % AIS2+=0.02 % AIS3+=0.00 %	Ribs	Max=0.89 % Max_{2nd}=0.83 % Max_{3rd}=0.69 %	1.5 %
Lumbar spine	-	-	-	-		Max=2.66 %	1.5 %
Pelvis	-	Quartile value of MPS distribution	Q95=2.6E-3 Q99=7.84E-3	AIS2+_45=7.0 % AIS2+_45=23.5 %		Max=3.18 %	1.0 %
		Deflection	0.70 mm	AIS2+=0.65			
R Thigh	-	$M_{Resultant}$				5.86 %	1.5 %
		Mid-femur	137.2 Nm	AIS3+=0.11 %			
		Mid-thigh	153.5 Nm	AIS3+=0.09 %			
		Dist-femur	133.7 Nm	AIS3+=0.29 %			
		Dist-thigh	153.6 Nm	AIS3+=0.28 %			
L Thigh	-	$M_{Resultant}$				3.88 %	1.5 %
		Mid-femur	104.5 Nm	AIS3+=0.02 %			
		Mid-thigh	113.6 Nm	AIS3+=0.01 %			
		Dist-femur	93.1 Nm	AIS3+=0.03 %			
		Dist-thigh	98.8 Nm	AIS3+=0.02 %			
R Knee	-	-	-	-		4.12 %	1.5 %
L Knee	-	-	-	-		0.10 %	1.5 %
R Leg	-	RTI				Tib:0.84 %	1.5 %
		Proximal	0.41	AIS2+=0.87 %		Fib:1.73 %	
		Distal	0.21	AIS2+=0.05 %			
		$M_{Resultant}$					
		Mid-Leg	82.7 Nm	AIS2+=0.04 %			
L Leg	Tibia & fibula Fracture (AIS2)	RTI				Tib:2.15 %	1.5 %
		Proximal	0.40	AIS2+=0.83 %		Fib:1.38 %	
		Distal	0.71	AIS2+=8.11 %			
		$M_{Resultant}$					
		Mid-Leg	158.7 Nm	AIS2+=1.46 %			
R Ankle	-	-	-	-		Max=1.39 %	1.5 %
L Ankle	-	-	-	-		Max=0.66 %	1.5 %
R Foot	-	-	-	-		Max=0.53 %	1.5 %
L Foot	-	-	-	-		Max=0.87 %	1.5 %

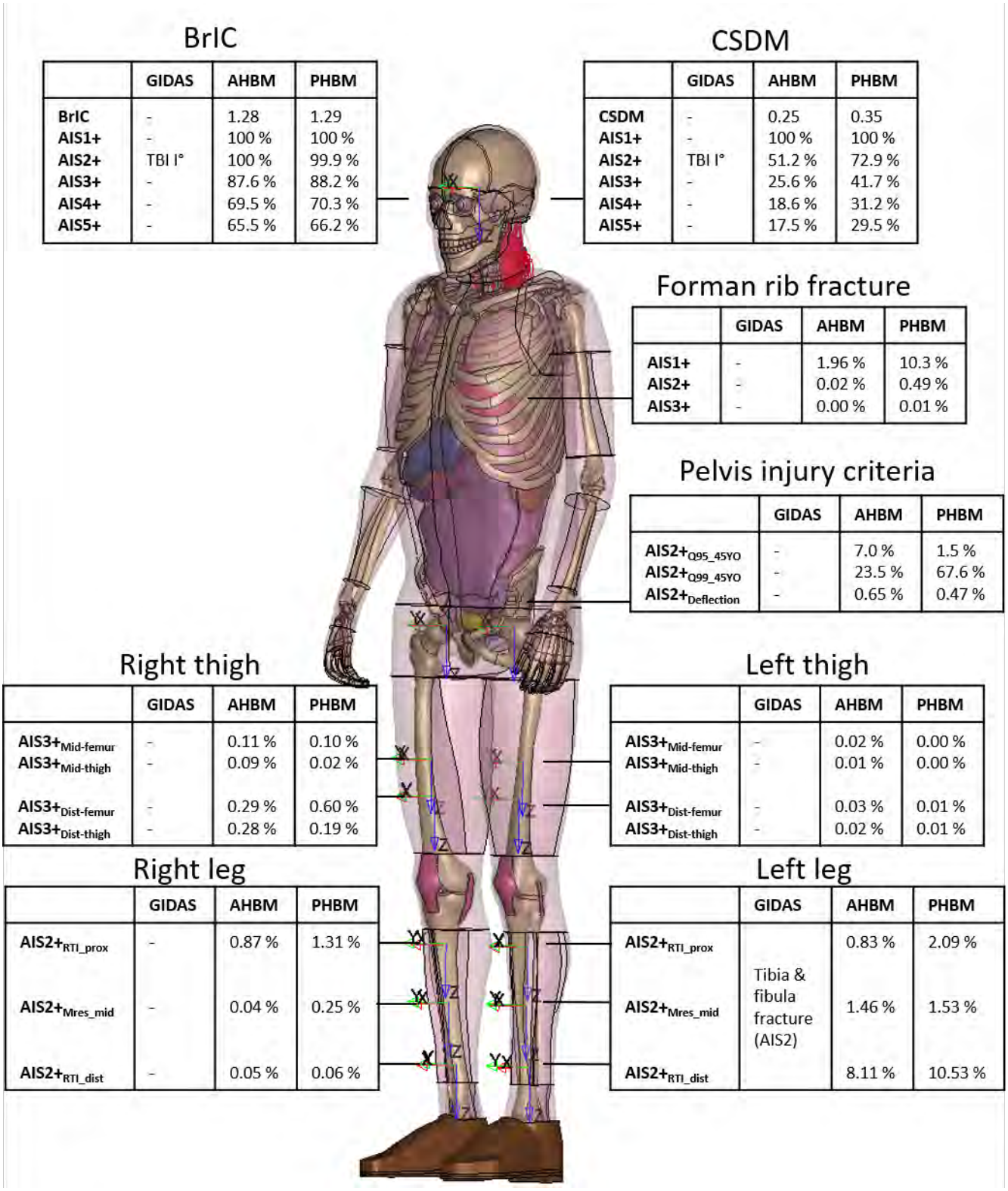

A-Fig. 7: GIDAS Case 1050918. Comparison of sustained injuries and probabilistic injury predictions by the AHBM and PHBM.

TABLE A-II

SUSTAINED INJURIES AND AHBM PREDICTIONS FOR GIDAS CASE 1170986

GIDAS		Probabilistic prediction			Deterministic prediction		
Region	Injury	Injury criterion	Injury value	Injury risk	Region	Max MPS	Threshold
Head	TBS I° (AIS2)	CSDM	0.43	AIS1+=100 % AIS2+=85.2 % AIS3+=54.6 % AIS4+=42.2 % AIS5+=40.0 %	-	-	-
	Graze forehead (AIS1)						
		BrIC	1.31	AIS1+=100 % AIS2+=100 % AIS3+=89.3 % AIS4+=72.0 % AIS5+=68.0 %			
Thorax	-	Forman		AIS1+=4.65 % AIS2+=0.09 % AIS3+=0.00 %	Ribs	Max=1.22 % Max_{2nd}=0.99 % Max_{3rd}=0.83 %	1.5 %
Lumbar spine	2 minimally dislocated bony fragments of the anterior edge of the L5 vertebra (AIS2)			-		Max=5.00 %	1.5 %
Pelvis	-	Quartile value of MPS distribution	Q95=7.04E-3 Q99=1.14E-2	AIS2+_45=73.7 % AIS2+_45=53.4 %		Max=3.29 %	1.0 %
		Deflection	0.59 mm	AIS2+=0.36			
R Thigh	-	$M_{Resultant}$				5.52 %	1.5 %
		Mid-femur	123.7 Nm	AIS3+=0.06 %			
		Mid-thigh	141.4 Nm	AIS3+=0.05 %			
		Dist-femur	112.8 Nm	AIS3+=0.10 %			
		Dist-thigh	124.6 Nm	AIS3+=0.08 %			
L Thigh	-	$M_{Resultant}$				3.90 %	1.5 %
		Mid-femur	142.5 Nm	AIS3+=0.14 %			
		Mid-thigh	150.8 Nm	AIS3+=0.08 %			
		Dist-femur	127.6 Nm	AIS3+=0.21 %			
		Dist-thigh	127.3 Nm	AIS3+=0.09 %			
R Knee	Graze	-	-	-		3.68 %	1.5 %
L Knee	Graze	-	-	-		0.46 %	1.5 %
R Leg	Graze	RTI				Tib:0.84 %	1.5 %
		Proximal	0.40	AIS2+=0.77 %		Fib:2.23 %	
		Distal	0.26	AIS2+=0.14 %			
		$M_{Resultant}$					
		Mid-Leg	95.4 Nm	AIS2+=0.08 %			
L Leg	Bruise	RTI				Tib:3.83 %	1.5 %
		Proximal	0.40	AIS2+=0.80 %		Fib:2.38 %	
		Distal	0.84	AIS2+=14.82 %			
		$M_{Resultant}$					
		Mid-Leg	223.5 Nm	AIS2+=9.85 %			
R Ankle	-	-	-	-		Max=0.76 %	1.5 %
L Ankle	Graze	-	-	-		Max=0.51 %	1.5 %
R Foot	-	-	-	-		Max=0.44 %	1.5 %
L Foot	Graze	-	-	-		Max=0.59 %	1.5 %

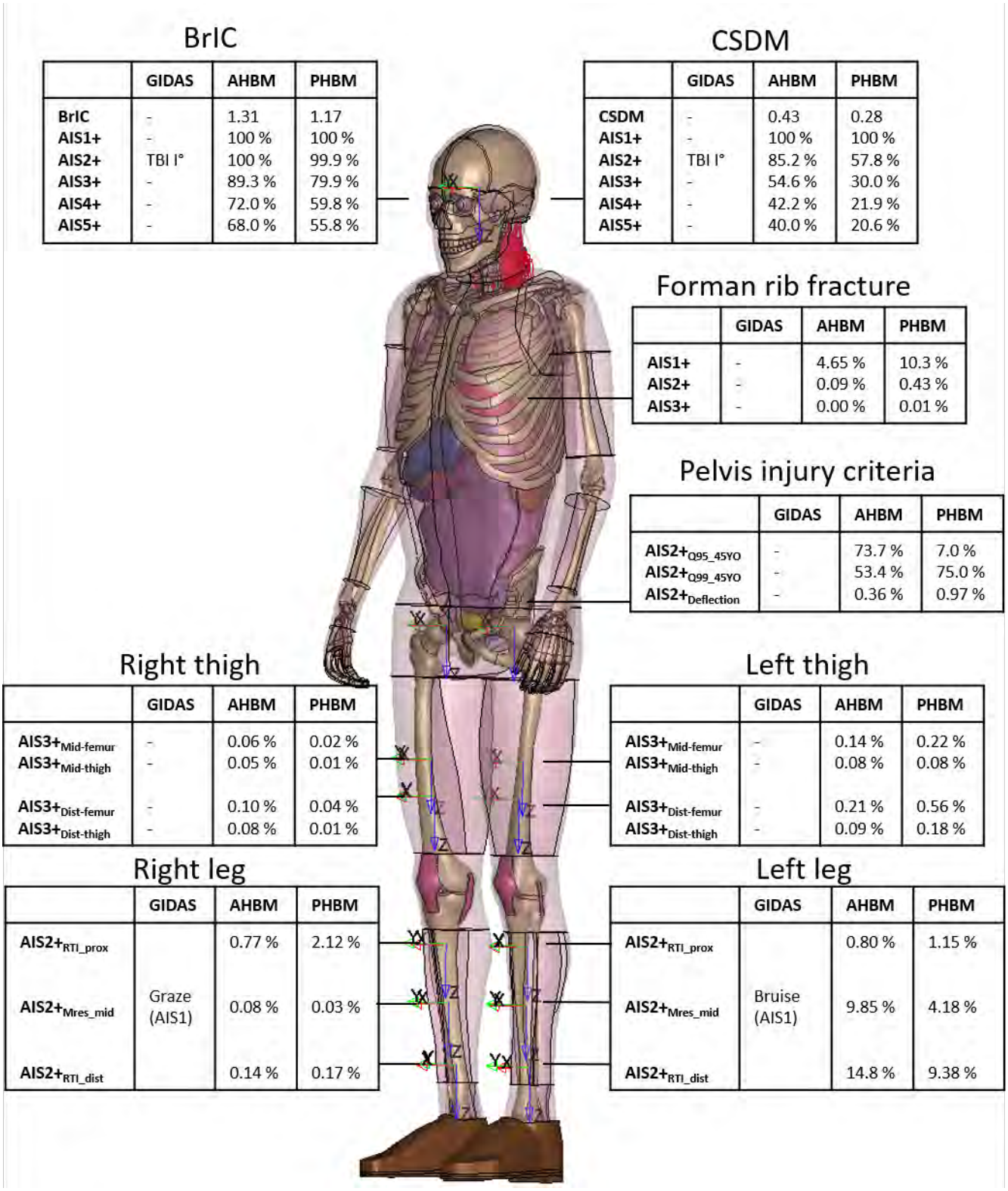

A-Fig. 8: GIDAS Case 1170986. Comparison of sustained injuries and probabilistic injury predictions by the AHBM and PHBM.

TABLE A-III

SUSTAINED INJURIES AND AHBM PREDICTIONS FOR GIDAS CASE 30090880

GIDAS		Probabilistic prediction			Deterministic prediction		
Region	Injury	Injury criterion	Injury value	Injury risk	Region	Max MPS	Threshold
Head	TBS I° (AIS2) Bruise (Os jugale, AIS1) Parietal wound head, L (AIS1) Nasal bone fracture (AIS1)	CSDM	0.18	AIS1+=99.9 % AIS2+=32.5 % AIS3+=15.0 % AIS4+=10.7 % AIS5+=10.0 %	-	-	-
		BrIC	1.04	AIS1+=100 % AIS2+=99.1 % AIS3+=68.9 % AIS4+=48.5 % AIS5+=44.8 %			
Thorax	Fracture L8, L9 (AIS2)	Forman		AIS1+=21.55 % AIS2+=1.69 % AIS3+=0.06 %	Ribs	Max=1.69 % Max_{2nd}=1.09 % Max_{3rd}=0.88 %	1.5 %
Lumbar spine	-	-	-	-		Max=3.21 %	1.5 %
Pelvis	Bruise (AIS1)	Quartile value of MPS distribution	Q95=6.53E-3	AIS2+_45=68.2 % AIS2+_65=82.6 %		Max=3.22 %	1.0 %
			Q99=1.04E-2	AIS2+_45=45.9 % AIS2+_65=61.4 %			
		Deflection	0.58 mm	AIS2+=0.34 %			
R Thigh	-	$M_{Resultant}$				5.80 %	1.5 %
		Mid-femur	190.6 Nm	AIS3+=0.84 %			
		Mid-thigh	206.4 Nm	AIS3+=0.56 %			
		Dist-femur	167.1 Nm	AIS3+=1.15 %			
		Dist-thigh	194.1 Nm	AIS3+=1.19 %			
L Thigh	-	$M_{Resultant}$				3.88 %	1.5 %
		Mid-femur	165.5 Nm	AIS3+=0.35 %			
		Mid-thigh	177.1 Nm	AIS3+=0.22 %			
		Dist-femur	151.2 Nm	AIS3+=0.62 %			
		Dist-thigh	163.6 Nm	AIS3+=0.41 %			
R Knee	-	-	-	-		3.82 %	1.5 %
L Knee	-	-	-	-		0.33 %	1.5 %
R Leg	-	RTI				Tib:0.90 %	1.5 %
		Proximal	0.37	AIS2+=0.59 %		Fib:2.05 %	
		Distal	0.40	AIS2+=0.81 %			
		$M_{Resultant}$					
		Mid-Leg	116.5 Nm	AIS2+=0.25 %			
L Leg		RTI				Tib:5.56 %	1.5 %
		Proximal	0.41	AIS2+=0.88 %		Fib:2.72 %	
		Distal	1.17	AIS2+=46.33 %			
		$M_{Resultant}$					
		Mid-Leg	243.8 Nm	AIS2+=15.63 %			
R Ankle	-	-	-	-		Max=1.32 %	1.5 %
L Ankle	-	-	-	-		Max=1.93 %	1.5 %
R Foot	-	-	-	-		Max=0.72 %	1.5 %
L Foot	-	-	-	-		Max=0.67 %	1.5 %

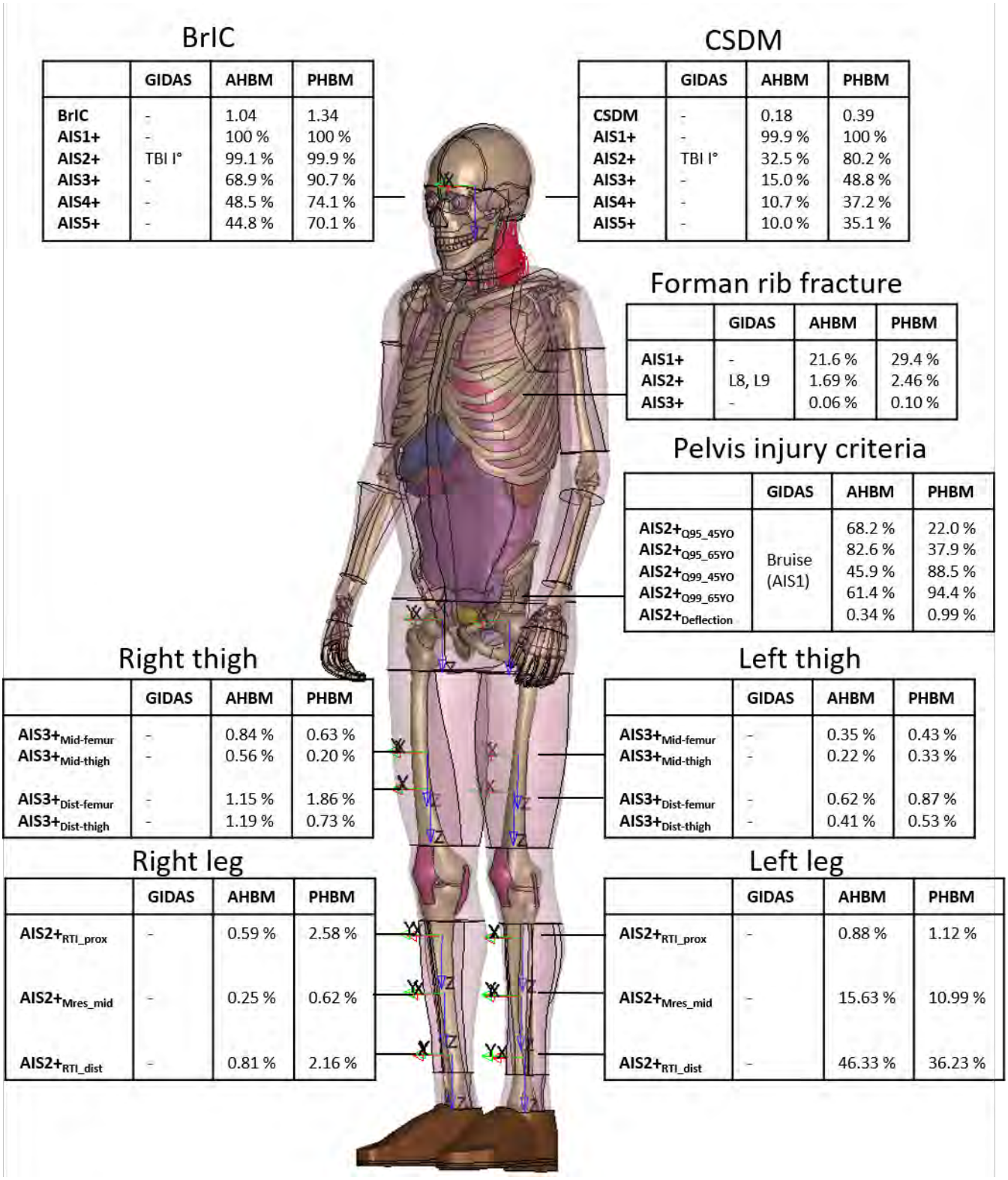

A-Fig. 9: GIDAS Case 30090880. Comparison of sustained injuries and probabilistic injury predictions by the AHBM and PHBM.

TABLE A-IV

AHBM INJURY PREDICTIONS FOR THE NO COLLISION SIMULATION

GIDAS		Probabilistic prediction			Deterministic prediction		
Region	Injury	Injury criterion	Injury value	Injury risk	Region	Max MPS	Threshold
Head	-	CSDM	0.00	AIS1+=0.00 % AIS2+=0.00 % AIS3+=0.00 % AIS4+=0.00 % AIS5+=0.00 %	-	-	-
		BrIC	0.05	AIS1+=8.34 % AIS2+=0.09 % AIS3+=0.02 % AIS4+=0.01 % AIS5+=0.01 %			
Thorax	-	Forman		AIS1+=0.03 % AIS2+=0.00 % AIS3+=0.00 %	Ribs	Max=0.29 % Max_{2nd}=0.27 % Max_{3rd}=0.22 %	1.5 %
Lumbar spine	-	-	-	-		Max=0.62 %	1.5 %
Pelvis	-	Quartile value of MPS distribution	Q95=4.31 E-3	AIS2+_45=34.3 % AIS2+_65=52.3 %		Max=3.18 %	1.0 %
			Q99=1.23 E-2	AIS2+_45=60.1 % AIS2+_65=74.1 %			
		Deflection	0.37 mm	AIS2+=0.07 %			
R Thigh	-	$M_{Resultant}$				3.11 %	1.5 %
		Mid-femur	53.6 Nm	AIS3+=0.00 %			
		Mid-thigh	36.5 Nm	AIS3+=0.00 %			
		Dist-femur	60.7 Nm	AIS3+=0.00 %			
		Dist-thigh	41.3 Nm	AIS3+=0.00 %			
L Thigh	-	$M_{Resultant}$				3.88 %	1.5 %
		Mid-femur	56.8 Nm	AIS3+=0.00 %			
		Mid-thigh	34.5 Nm	AIS3+=0.00 %			
		Dist-femur	57.3 Nm	AIS3+=0.00 %			
		Dist-thigh	40.4 Nm	AIS3+=0.00 %			
R Knee	-	-	-	-		0.34 %	1.5 %
L Knee	-	-	-	-		0.15 %	1.5 %
R Leg	-	RTI				Tib:0.74 %	1.5 %
		Proximal	0.25	AIS2+=0.11 %		Fib:0.75 %	
		Distal	0.10	AIS2+=0.00 %			
		$M_{Resultant}$					
		Mid-Leg	25.7 Nm	AIS2+=0.00 %			
L Leg		RTI				Tib:0.81 %	1.5 %
		Proximal	0.25	AIS2+=0.12 %		Fib:1.04 %	
		Distal	0.10	AIS2+=0.00 %			
		$M_{Resultant}$					
		Mid-Leg	29.1 Nm	AIS2+=0.00 %			
R Ankle	-	-	-	-		Max=0.20 %	1.5 %
L Ankle	-	-	-	-		Max=0.31 %	1.5 %
R Foot	-	-	-	-		Max=0.36 %	1.5 %
L Foot	-	-	-	-		Max=0.51 %	1.5 %

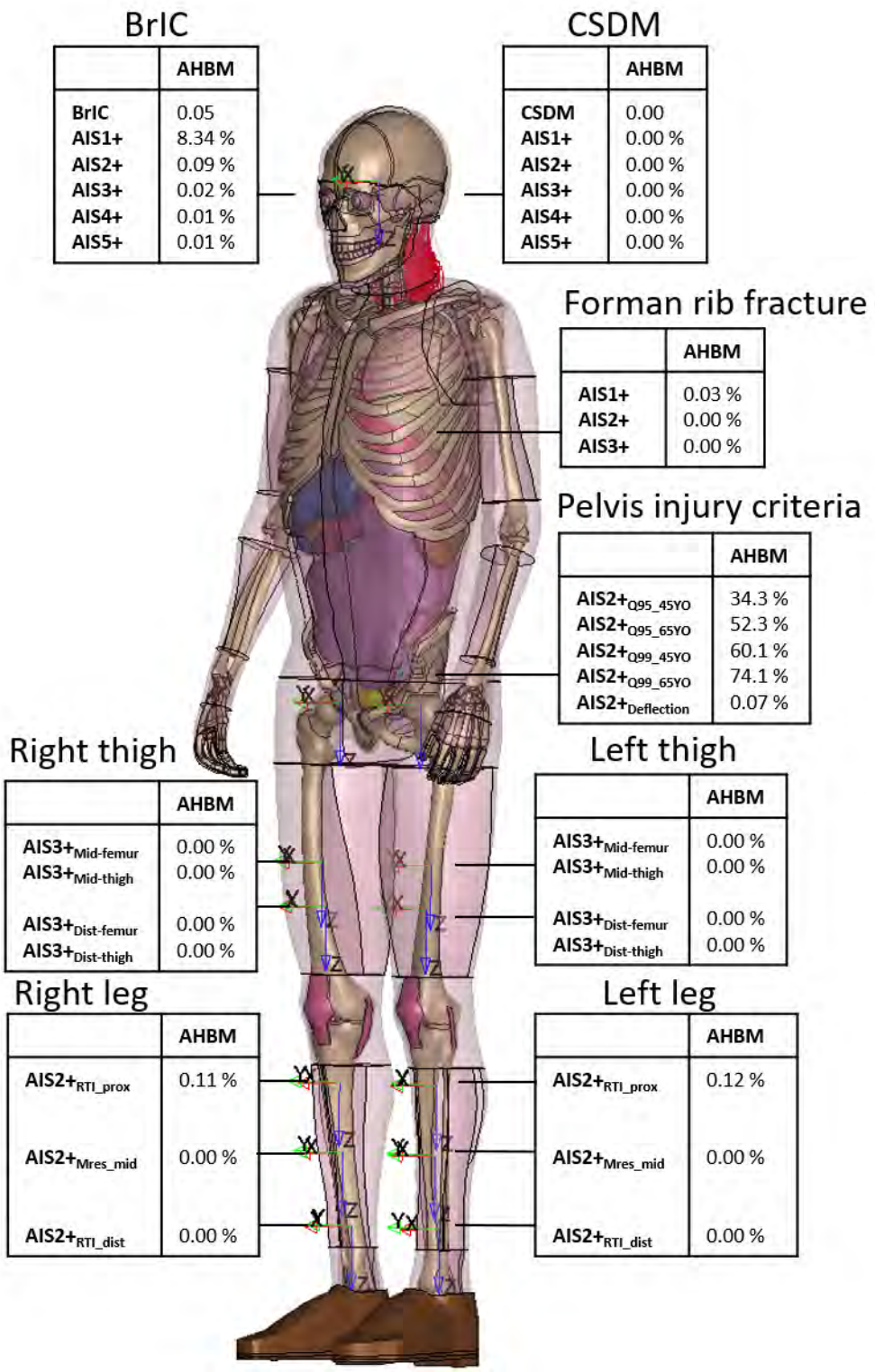

A-Fig. 10: No collision simulation. Summary of the probabilistic injury predictions by the AHBM. Pelvis injury risks were calculated based on the original calculation method [52].

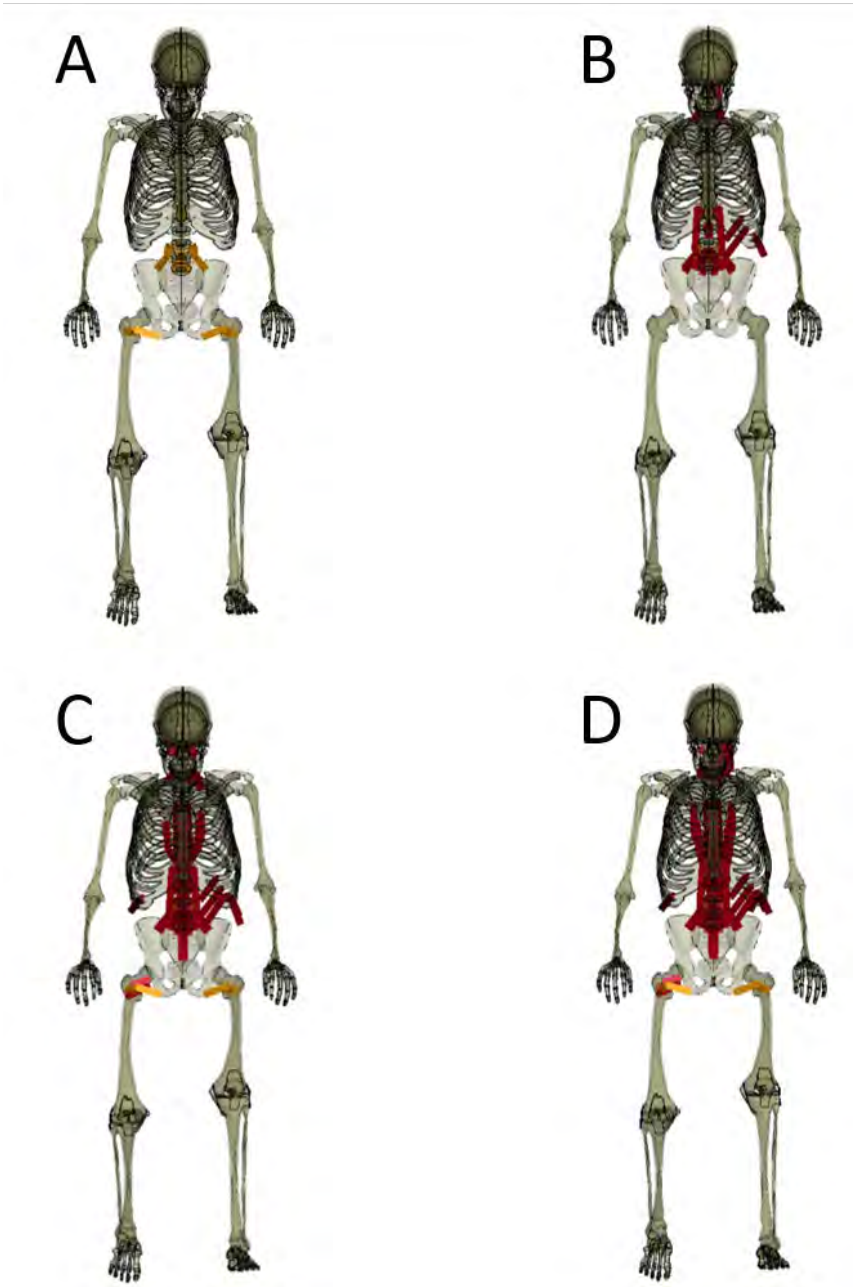

A-Fig. 11: Visualisation of muscles showing strain injury within the THUMS cyclist AHBM. A) No collision simulation, B) #GIDAS 1050918, C) #GIDAS 1170986, and D) #GIDAS 30090880. Baseline injuries are denoted in orange, additional injuries caused by the impact are marked in red.

TABLE A-V

JOINT ANGLE OFFSET OF THE DEFAULT THUMS PEDESTRIAN MODEL, AS DETERMINED WITH THE MB HBM AND SUBTRACTED FROM THE POSE ESTIMATION RESULT FOR PRIMER REPOSITIONING

Joint Title	PHI/X-Angle [°]	THETA/Y-Angle [°]	PSI/Z-Angle [°]
Left Hip Joint	2.9	-3.1	3.47
Right Hip Joint	-2.9	-3.1	-3.47
Left Shoulder Joint	-9.13	-1.0	-9.8
Right Shoulder Joint	9.13	-1.0	9.8
Left Forearm Joint	-	26.0	-
Right Forearm Joint	-	26.0	-
Left Wrist Joint	-	5.0	-
Right Wrist Joint	-	5.0	-